AXISYMMETRIC INSTABILITY IN A NONCIRCULAR TOKAMAK

BY

BRUCE LIPSCHULTZ

A thesis submitted in partial fulfillment of the
requirements for the degree of

DOCTOR OF PHILOSOPHY

(Physics)

at the

UNIVERSITY OF WISCONSIN - MADISON

1979

ACKNOWLEDGEMENTS

I thank Stewart Prager, and am indebted to him, for the many invaluable discussions we have shared.

For his interest in my research and discussions of this thesis, I thank Clint Sprott. Others that provided helpful discussions were Dr.'s Kerst and Post. I also would like to thank Thomas Osborne for his help with early experiments and the flux plot program.

The work of Thomas Lovell, Bob Vallem, and their technical crew with the experimental equipment has been invaluable.

Last, and most importantly, I thank my wife Shelley for her patience and understanding during my graduate career, and assistance with this thesis.

TABLE OF CONTENTS

AXISYMMETRIC INSTABILITY IN A NONCIRCULAR TOKAMAK

Bruce Lipschultz

Under the supervision of

Professor J.C. Sprott and Assistant Professor S.C. Prager

The stability of dee, inverse-dee and square crossection plasmas to axisymmetric modes has been investigated experimentally in Tokapole II, a tokamak with a four-null poloidal divertor. Experimental results are closely compared with predictions of two numerical stability codes--the PEST code (ideal MHD, linear stability) adapted to tokapole geometry and a code which follows the nonlinear evolution of shapes similar to tokapole equilibria. Experimentally, the square is vertically stable and both dee's unstable to a vertical nonrigid axisymmetric shift. The central magnetic axis displacement grows exponentially with a growth time~10^3 poloidal Alfven times~ plasma L/R time. Proper initial positioning of the plasma on the midplane allows passive feedback to nonlinearly restore vertical motion to a small stable oscillation about the center. Experimental poloidal flux plots are produced directly from internal magnetic probe measurements. The PEST code, ignoring

passive feedback, predicts all equilibria to be vertically unstable with the square having the slowest growth. With passive feedback, all are stable. Thus experiment and code agree that the square is the most stable shape, but experiment indicates that passive feedback is partially defeated by finite plasma resistivity. In both code and experiment square-like equilibria exhibit a relatively harmless horizontal instability.

J. C. Sprott

S. C. Prager

CHAPTER I

INTRODUCTION

A. GENERAL OVERVIEW

The deleterious effect of impurities in tokamak plasmas has stimulated investigation of poloidal divertor configurations. The necessarily noncircular shape of these equilibria is also advantageous with respect to q[1] and β-limited MHD instabilities[2,3]. Unfortunately any deviation of an equilibrium from a circular shape may permit the plasma to be unstable to axisymmetric displacements, with toroidal mode number n=0. The poloidally asymmetric placement of shaping rings and walls necessary to establish a noncircular plasma shape in turn creates nonuniform attractions to the plasma current. The plasma, if perturbed, moves in the direction of the minimum in the accompanying poloidal field. Unlike kink and localized interchange modes, the axisymmetric instability cannot be controlled by increasing the toroidal field or reducing the plasma current.

Unfortunately, the conceptual simplicity of the axisymmetric instability does not translate into calculational simplicity. The importance of this mode has given rise to a fairly large amount of linear theory – mostly for idealized displacements and analytic equilibria [4-12]. Recently nonlinear evolution of the instability has been followed numerically [13]. Axisymmetric displacement of dee and elliptical plasmas has been deduced in a few experiments from magnetic probes external to the plasma[14-17]. The plasma shape in these experiments has been inferred from comparison of these same external magnetic signals with output from equilibrium computer codes. The numerical modeling of the axisymmetric instability, cited above, has apparently not been specifically applied to any of these experiments; an unfortunate gap exists between a fairly well developed theory and experiments performed.

The intent of this thesis is twofold. First, to report direct experimental observation of the axisymmetric instability in dee, inverse-dee and square shaped cross sections. Second, to compare these experimental observations with a stability code written for the actual experimental geometry. This experiment has been performed in the Wisconsin Tokapole II[18,19], a

Tokamak with a four-null poloidal divertor. Experimental magnetic flux plots for the aforementioned range of equilibria are produced, from magnetic probe measurements in the plasma interior, in detail equivalent to that provided by computer calculations. Conclusions, as to growth rates and passive stabilization, can be drawn from the time evolution of these experimental flux plots and compared with two numerical codes which closely reflect the experimental machine. The PEST code[20], which has been adapted to the Tokapole machine geometry, predicts the linear stability . The effects due to external conductors are included by appropriate vacuum modifications[21,22]. A nonlinear time dependent code, PATENT[13,23], although applied to the PDX[24] machine only, provides qualitative stability predictions and modeling of the plasma shape as a function of time. Because of the wide seperation of time scales in this experiment (e.g. Alfven, plasma and ring L/R times) many qualitative conclusions about passive stabilization can be drawn which are relatively machine independent. Qualitative comparison can also be made between experimental results and related models in the literature[19].

Several parameter variations are possible both

experimentally and numerically. For example, proper positioning of the four field shaping rings allows equilibria to be varied from dee through square to inverse-dee shaped. The dee and inverse-dee are vertically unstable when not precisely centered on the machine midplane. When vertical stability is achieved, these shapes are still horizontally unstable. The square is vertically stable even if not precisely positioned. However, this shape is also horizontally unstable. Since the horizontal instability saturates it is less harmful than the vertical displacements exhibited in the dee and inverse-dee. The vertical movement continues unrestrained towards the x-point (poloidal field null on the separatrix). Predictions of the PEST code for relative stability of these equilibria agree with experiment. Experimentally, the magnetic axis can be positioned above, below or exactly on the midplane. In both the PATENT code and experiment the plasma is seen to correspondingly move up, down or oscillate about the midplane. Both experimentally and from the nonlinear code we find the growth of the instability to be exponential in time. Ideal MHD predicts the growth time, in the absence of external conductors, to be $\sim T_a$, the poloidal Alfvén time. Experimentally, vertical and horizontal growth times are $\sim 10^3 T_a$. Passive feedback

apparently increases T_g, the growth time, from T_a to roughly the plasma L/R time. The effect of passive feedback from rings and walls is studied experimentally by changing the plasma resistivty and by varying the initial position of the magnetic axis. The instability growth time varies inversely with plasma resistivity. Stability can be numerically studied with or without rings or walls to evaluate their effect on passive stabilization.

In section B of this chapter an attempt is made to give the reader an intuitive feel for the physical nature of axisymmetric instabilities. Chapter II includes a description of the experimental machine (II.A) and techniques (II.B), as well as a review of previous (II.C) and present (II.D-F) experimental results. Chapter III is devoted to theory. After a review of previous theoretical work (III.A), the numerical codes used in this study are described (III.B-D) and their predictions reviewed (III.E-F). Experimental and theoretical results are discussed and compared in Chapter IV with a summary in table 1.

B. Physical Intuition

The physical nature of the axisymmetric instability
can be illuminated through intuitive means. At first we
will assume that currents in the plasma and external
conductors are fixed. Also, for simplicity, we will
discuss linear as opposed to toroidal geometry.
Allowance for toroidal curvature introduces a force
produced by the inductive interaction of the plasma
current with its self magnetic field. This force tends
to increase the plasma major radius and is different in
nature from the axisymmetric instabilities discussed
here.

It is illustrative to study a stable equilibrium and
then relate what actions must be taken to create an
unstable one. This simple situation of a linear tokamak
plasma is illustrated in figure 1a. We see, for this
circular shape with return current at infinity, there is
no preferred direction, i.e. there are no currents or
magnetic fields for the plasma current to interact with.
Thus it is neutrally stable with respect to a rigid
displacement; given a perturbation it will keep
travelling at a constant velocity. This neutral
stability to displacements can be modified to instability

Figure 1: Illustration of the relation between deformation and stability in a linear geometry. All three plasma crossections include 'toroidal' current into the paper. a) Neutrally stable circular plasma extending into paper. b) Elliptical plasma deformed from circle by currents I_1 & I_2. The attractive forces, F_1 & F_2, between the plasma current and each shaping rod are balanced. c) Same elliptical plasma displaced vertically. F_1 & F_2 are no longer balanced – vertical displacement grows.
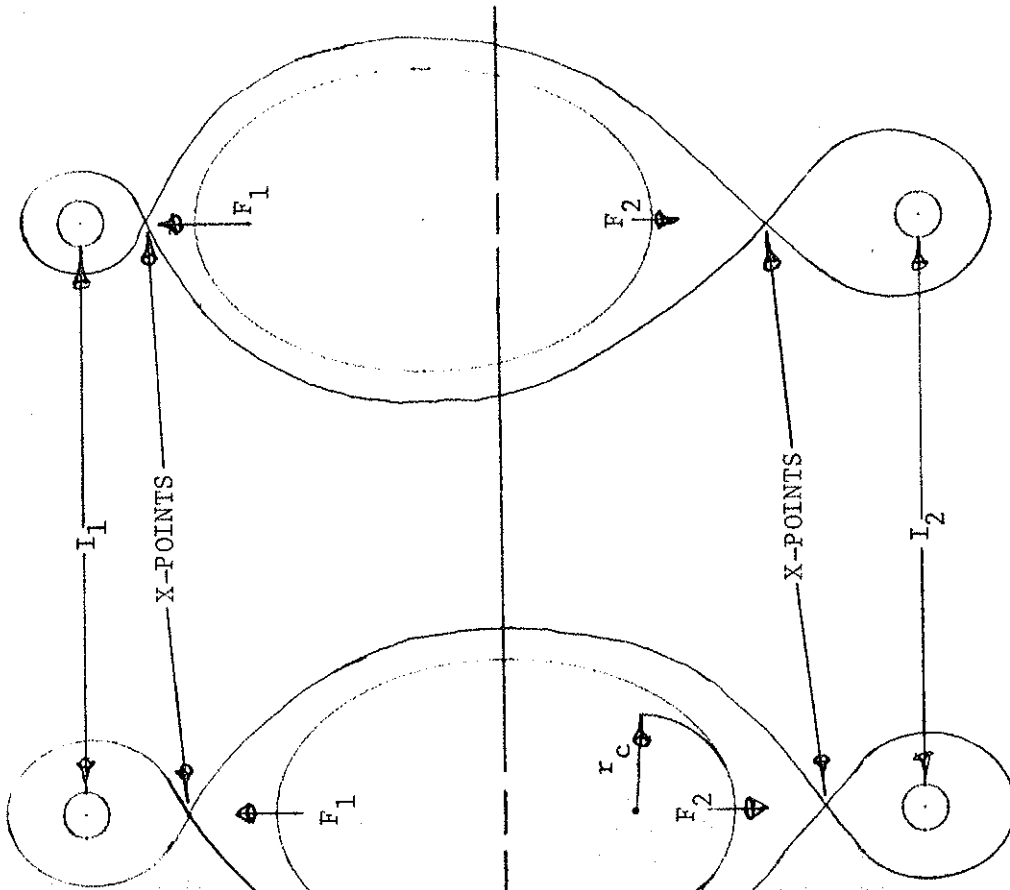
8

a)

b)

c)

F_1

F_2

F_1

F_2

r_c

I_1

I_2

X-POINTS

X-POINTS
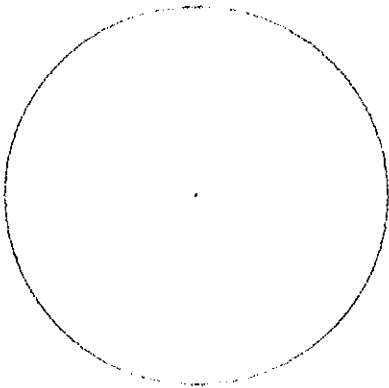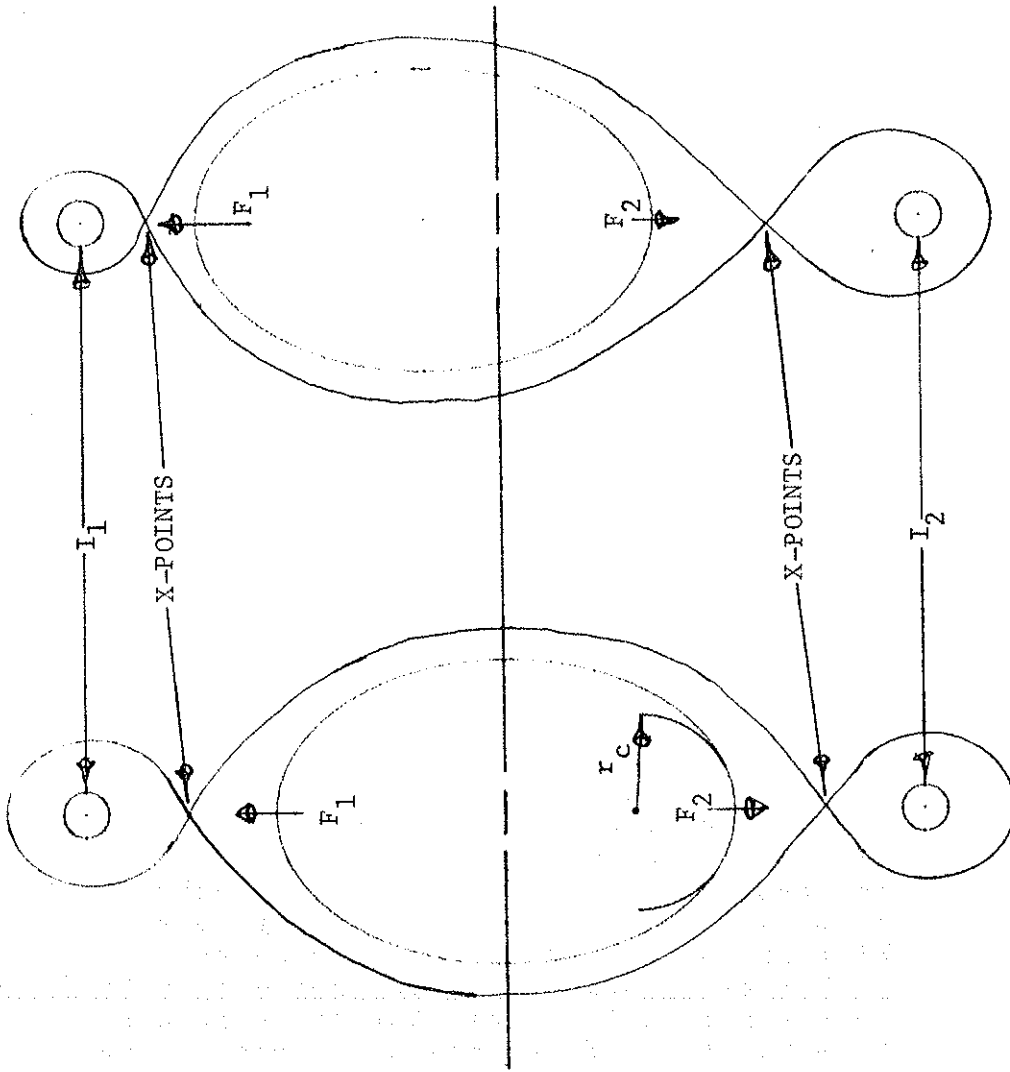
by deforming the plasma to a noncircular shape using external currents (fig. 1b). Here the plasma current can interact with the shaping currents, absent in the circular case. This attraction is the characteristic driving force of what is generally called the vertical 'axisymmetric' instability. The word 'axisymmetric' in this linear situation connotes an axially symmetric movement of the entire plasma column, with axis into the paper. When this ellipse is positioned precisely between the two shaping currents, the forces F_1 and F_2, between the plasma and shaping currents, are balanced. If the ellipse is perturbed vertically away from this point, F_1 and F_2 become unbalanced, and instability growth ensues (fig. 1c). No great leap of the imagination is needed to see that increasing the deformation (ellipticity) will increase the instability growth rate. The attraction is greater because: 1. The shaping currents are larger and, 2. The plasma is in closer proximity to these currents. The increase in deformation can best be characterized by a decrease in the poloidal field radius of curvature; r_c, near the x-point (see fig. 1b).

This same prescription: decreasing r_c ~ increasing deformation ~ plasma more unstable to displacements, can be applied to other shapes. In the presence of an

octupole field (fig. 2a), a square cross section plasma will be more stable to displacements in the direction of an octupole current than either a dee or inverse-dee. The latter two shapes are equivalent in a linear geometry. In comparison to the square, the dee of equivalent current is closer to either pair of z-symmetric shaping current conductors. Also these closer currents must be increased to initially create the dee. Thus the dee will experience greater attractive forces. The more unstable shape again has the greater deformation or smaller r_c. The dee, when perturbed upward (downward) will move towards the upper (lower) closest octupole current. The attractive force increases as the dee moves closer. Figure 2b illustrates the situation. Although this is what is generally denoted a vertical instability a more apt name that I will use in this discussion is x-point instability. The attractive force that drives this instability is always between two like currents that generate a field null (x-point).

The role of the plasma current distribution is important to these instabilities. A flat current distribution is more unstable than a parabolic profile for approximately the same plasma shape and total current. There is more plasma current in closer

11

a)

b)

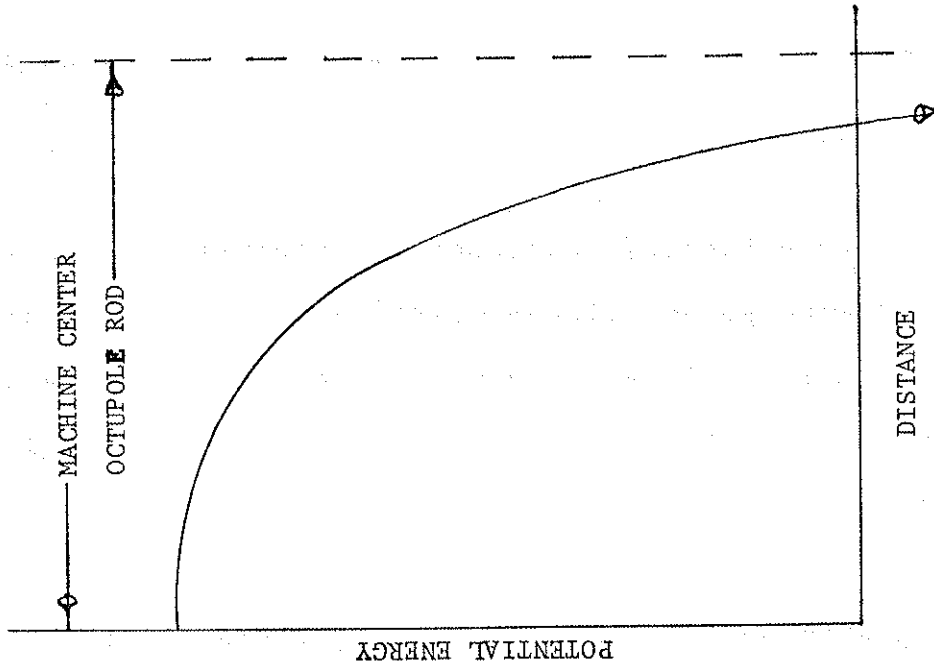MACHINE CENTER

OCTUPOLE ROD

POTENTIAL ENERGY
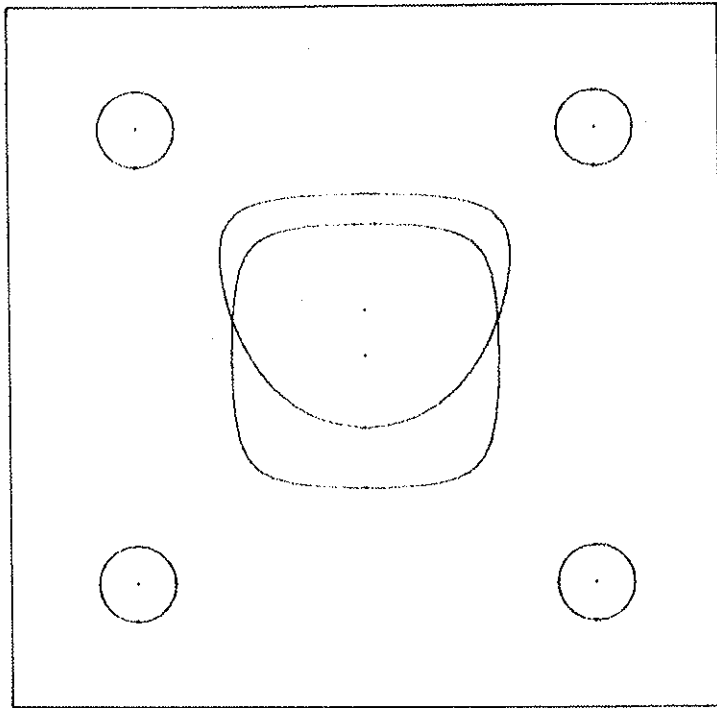
DISTANCE

Figure 2: A further illustration of the x-point
instability in a linear geometry. a) The inverse-dee
is closer to shaping rods than square. b) Potential
energy vs. distance to the attracting rod.

proximity to the shaping currents. The attractive force is $\propto 1/r$, where r is the relative distance between the currents involved.

Understanding horizontal (equivalent to vertical direction in a linear device) displacements is not as straightforward as the x-point instablity. If a toroidal current filament were placed centrally in a linear octupole field, it would be horizontally stable. Designating the toroidal direction as into the paper, then examination of the $\underline{I}_{fil} \times \underline{B}_{pol}$ force at points along the midplane, for this test current and vacuum poloidal magnetic field, reveal a restoring force that increases monotonically with minor radius. A potential energy curve, illustrating this effect, is drawn as a function of distance along the midplane in figure 3a. Note this curve is shallower than that for the x-point direction (fig. 2b) because the octupole rods are closer to machine center than the image currents that represent the wall. A plasma is not a current filament: we must take into account the sum of forces over the plasma cross section. Furthermore, the plasma is a cohesive entity described by the MHD equations. Figure 3b exhibits this force field, experienced by a filament test current, for one quadrant of the octupole field. The
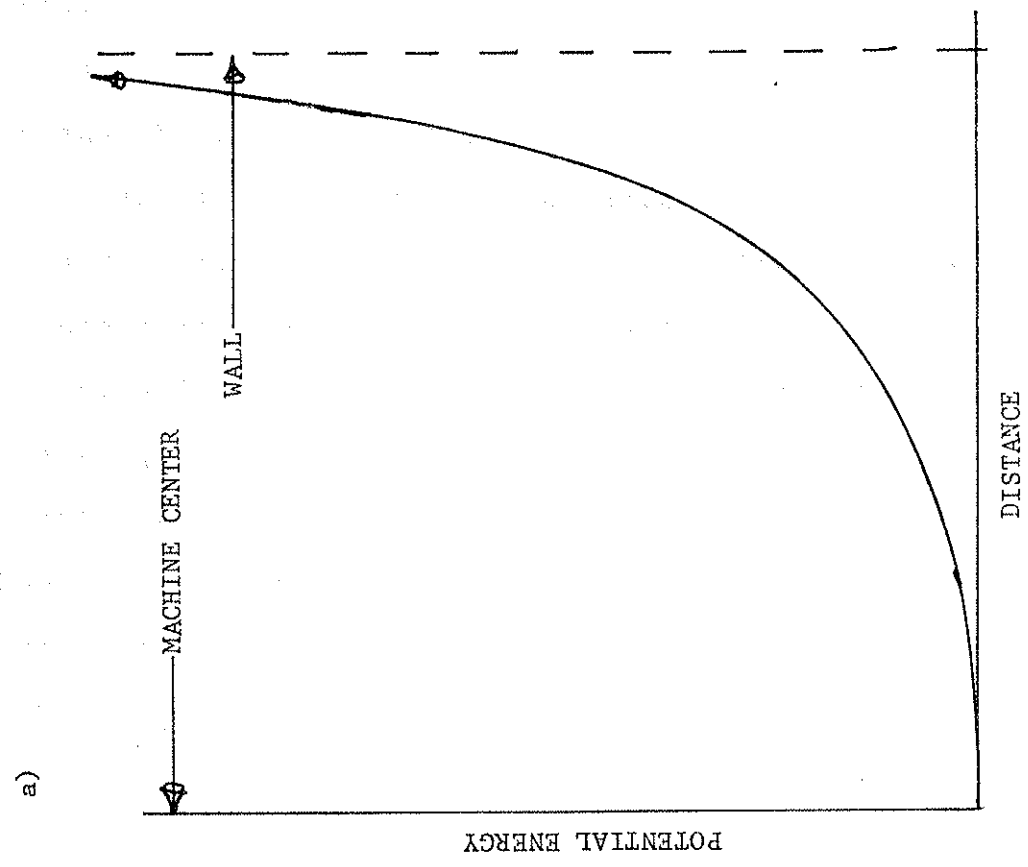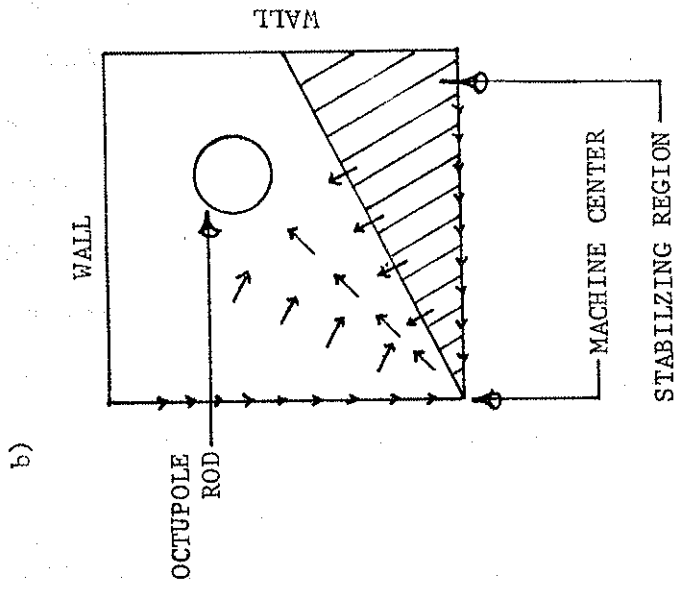
Figure 3: Illustration of the horizontal instability in an octupole geometry. a) Potential energy vs. distance to the wall. b) Force field of a filament test current in one quadrant of octupole. Shaded area has a horizontally stabilizing influence.

complete flux plot from which this figure is derived is shown in fig. 5. Since, in linear geometry, all quadrants are equivalent only one is shown in fig. 3b. The area that repels horizontal movement is shaded. Comparing the square shape, placed at machine center, to the inverse-dee, displaced to the right, the square contains less of the horizontally stabilizing region than the inverse-dee. Therefore, the square is least stable to horizontal as opposed to x-point displacements.

Up until now, we have treated the plasma and external conductors as having fixed currents during displacements. If the currents involved are allowed to react to the plasma motion, passive stabilization can occur. Let us first treat the idealized case of two parallel currents with the constraint that their total flux be held constant during movement (fig. 4). Ignoring reconnection (i.e. for an infinitely conducting plasma at the x-point), if they are allowed to move towards each other, field lines will be compressed and the integral of $\underline{B} \cdot \underline{dl}$ around each rod will increase. Antiparallel currents will be correspondingly induced to keep this integral a constant. Thus the currents are reduced causing the attractive force, $2I_1 I_2 / r_{12} c^2$, and growth rate to decrease. This effect, of induced
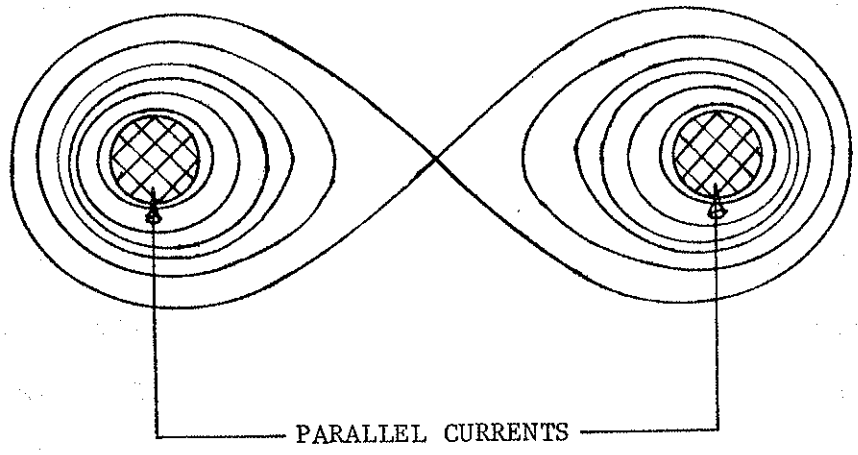
PARALLEL CURRENTS

Figure 4: Two parallel linear (into paper) currents with accompanying quadrupole magnetic field.

currents slowing the movement, is termed passive stabilization.

There are two complicating factors that can affect the efficiency of passive stabilization. The first to be discussed is finite resistivity in the conductors. Compressed flux can be pushed through the rods on a soak-in time scale T_{soak} proportional to the square root of conductivity. The net effect is that induced stabilizing currents will decay over time. Thus, if a movement (instability) could be stabilized by rods of infinite conductivity, then allowing finite resistivity enables the instability to grow with a rate~$1/T_{soak}$.

The other factor in passive stabilization is the presence of plasma. In a vacuum field, lines can reconnect instantly. In the presence of plasma, line reconnection occurs at a rate $\propto 1/T_{res}$. T_{res} is the characteristic resistive decay time of the plasma. Thus, additional flux compression can occur, slowing the instability growth rate.

If we apply the concept of passive stabilization to the case of the x-point unstable dee in an octupole field, the plasma and nearest rod are the primary

currents involved. There is also, of course, plasma at the x-point. Some passive stabilization will occur but full stabilization is not neccesarily possible. If we bring into this discussion the effect of conducting elements other than those primarily involved, then passive stabilization will be more effective. Flux decompression, with accompanying induced attractive currents, will occur in the other conductors (e.g. the other three rods and opposite walls). The efficiency of induced effects will not only be determined by the characteristic resistive decay time scales involved, but on the amount and proximity of induced currents as well. The dee is in closer proximity to fewer rings and walls than the square of equivalent total current. Therefore, passive stabilization will be more effective for the square than for the dee. In either case, if the plasma is not completely stabilized, then the growth time will be slowed to the order of the minimum of the resistive time scales involved.

Not discussed, heretofore, is the relation of the 'toroidal' field to the axisymmetric instability. Intuitively, it must play a much smaller role than the poloidal field. The deformation will stretch the poloidal field on the order of a minor radius-scale

length. On the other hand, the toroidal field is only slightly deformed while the entire field line is being pushed out of the way, either up or down. There _may_ be some horizontal stretching to this movement but it is on the order of the major radius. Thus, the displacement divided by the scale length involved is smaller for the toroidal field. In addition to this small contribution of the stretched toroidal field, there is the effect of its gradient introduced by toroidality. In equilibrium, by definition, the $\underline{J}_{pol} \times \underline{B}_{tor}$ force is balanced everywhere by $\underline{J}_{tor} \times \underline{B}_{pol}$ (for low pressure). When the plasma becomes unstable, this condition may perhaps no longer hold. Examination of the $\underline{J}_{pol} \times \underline{B}_{tor}$ force near the principal x-point involved, shows that the force increases as major radius R decreases. The introduction , therefore, of toroidal curvature can perhaps differentiate between the two dee's making the dee slightly more unstable than the inverse-dee.

In summary, through the application of basic physical concepts, we can see that increased deformation (decreasing r_c) indicates a shape to be relatively more unstable toward x-point displacements. This implies the square is more stable than the dee or inverse-dee. Passive feedback stabilization can either completely

stabilize this movement or at least slow its growth to
the resistive time scales involved. Its effectiveness
should be greater for the square than for the dee's. The
relative stability of these shapes becomes reversed when
discussing horizontal displacements. The effect of
toroidal field, though all important for higher n
(toroidal mode number) instabilities, has only a minor
influence on the stability of the axisymmetric modes
(n=0).

CHAPTER II

EXPERIMENT

A. Machine Description

The Tokapole II device[18], on which these experiments
were performed, has a 50 cm. major radius square
cross section (44 x 44 cm.) vacuum chamber. The vacuum
magnetic flux plot is that of an octupole (fig. 5a),
which provides vertical and horizontal fields to center
the discharge. The octupole vacuum poloidal field is
produced by inductively driving, through an iron core
linking the toroid, four 5 cm. diameter copper toroidal
rings. These rings can carry up to a total of 700 kA,
and are each supported by three copper-beryllium rods.
While the chamber is under vacuum the rings can be moved
vertically ±5mm. by external means. When plasma current
is driven toroidally through the octupole null, a tokamak
with a four-null divertor is generated (fig. 5b).

Electrical characteristics are shown in figure 6.
The current in an outer ring rises sinusoidally to 45 kA
(fig. 6a). A 1 msec. pulse of 10 kW. 8.8 GHz

Figure 5: Numerical poloidal flux plots
(major axis to left). a) Without plasma.
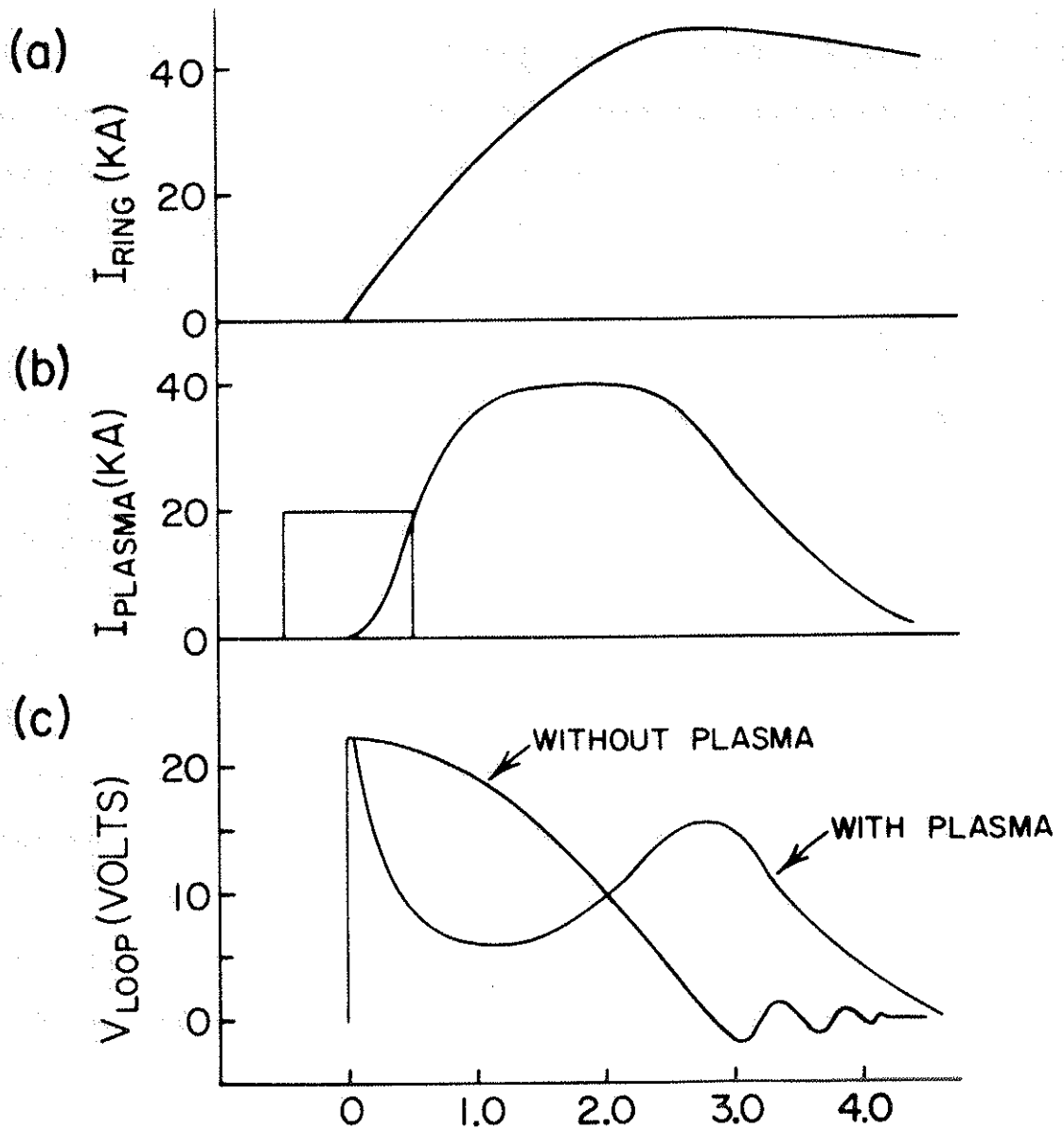b) With plasma. Each tic mark indicates
2 cm.
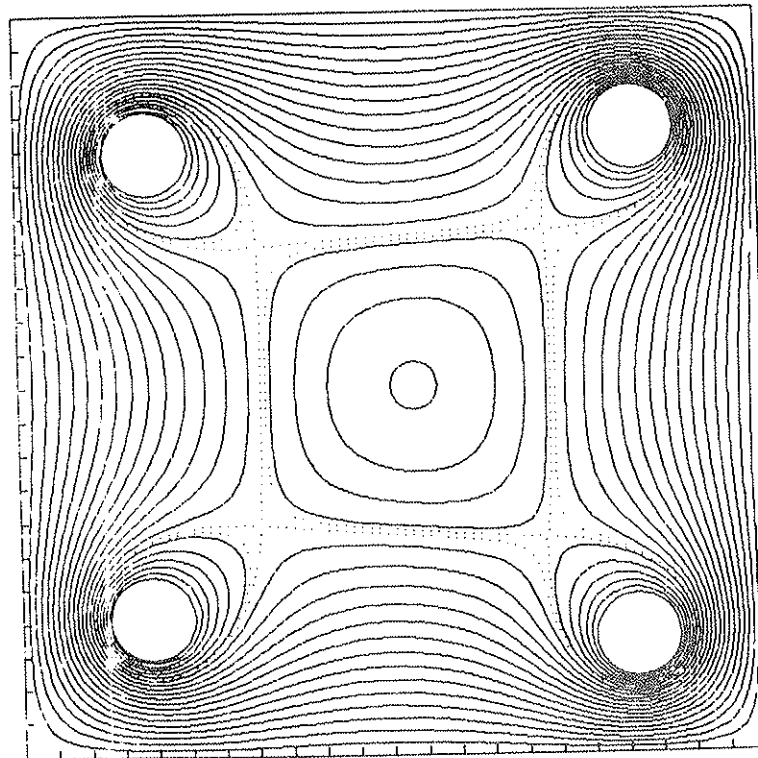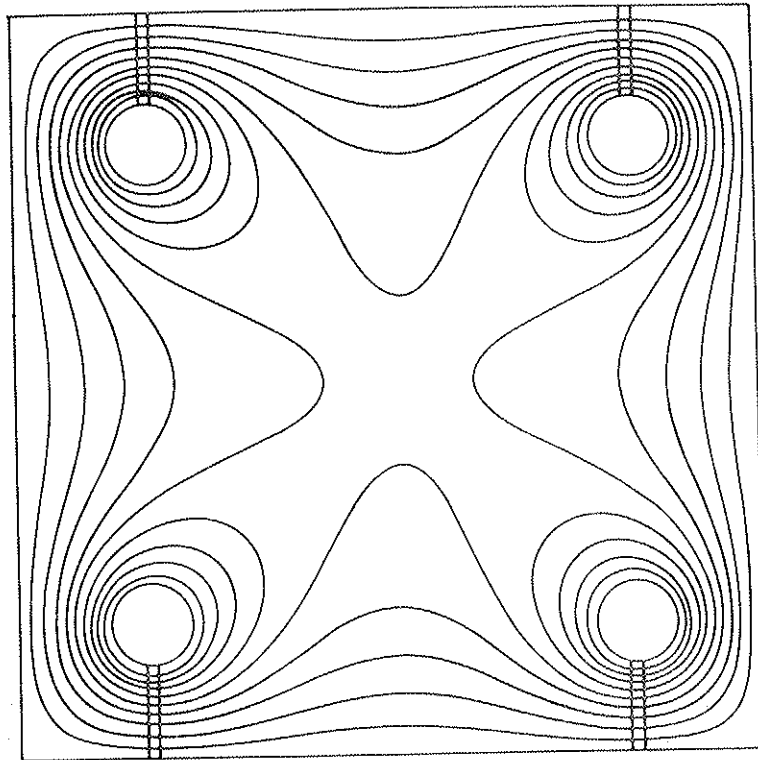
Figure 6: Electrical characteristics. Time, in ms., is given on abscissa. a) Current in an outer ring vs. time. Also shown is a 10 kW, 8.8 GHz, 1 ms. microwave preionization pulse. b) Plasma current. c) Loop voltage at machine center with and without plasma.

microwaves is used for preionization (fig. 6b). The plasma current is induced by the same source as the ring current. The value for the total toroidal plasma curent is inferred from measurements of the poloidal field transformer primary current and loop voltage, at the wall, employing a simple model treating the plasma and rings as coupled inductors[25,26]. The current inside the separatrix is also calculated from measured magnetic flux plots. The peak total plasma current is ~ 40 kA with ~ 4 msec pulse length (fig. 6b). The toroidal field is effectively constant during the experiment at a value of 3.2 kG at machine center, with capability of up to 8.5 kG. The vacuum toroidal loop voltage (fig. 6c) at machine center decays as a cosine to zero in ~ 3 msec and is then crowbarred. In the presence of plasma the loop voltage is depressed during plasma current rise and enhanced during current decline due to the back EMF self-induced by the plasma current. Peak electron temperatures are ~ 100 eV surmised, with ~ 25% accuracy, from modeling of the time evolution of a set of impurity lines (e.g. OI-OVI). The electron density is ~ 10^{13} cm^{-3} as measured by microwave interferometry and Langmuir probes. The ion temperature varies from 20-70 eV as determined by charge-exchange analysis and from the doppler broadening of He II.

B. Experimental Techniques

The basic information without which this research would not be possible is the poloidal magnetic flux plot. The tool used for obtaining a flux plot is the 'Ḃ' probe — so termed because the output is proportional to the time derivative of magnetic flux at the probe tip. The 'Ḃ' probes used in these experiments consist of two 40 turn, 4x4x5 mm coils of wire, located at the sealed end of a 1/4 inch tube. The coils are wound on top of each other and have normals parallel and perpendicular to the probe length. The orientation allows both components of poloidal magnetic field to be resolved. The frquency response of this probe varies between 100 kHz. and 1 mHz. depending on the exact number of turns and areas of the coils.

After passive integration, each probe signal is digitized and stored by computer. To correct for probe misalignments at a given point, a discharge with only the toroidal field is stored and subtracted from the data with both magnetic fields and plasma. After this

correction, the probe signal every 50µs, for 4 msec., is stored on floppy disk for further analysis.

The expression used to calculate the poloidal flux, ψ is

$$\psi = \int_0^r dr'\ 2\pi(R_0+r')B_{perp}(r') \tag{2.1}$$

where R_0, r' and B_{perp} are the major radius of the magnetic axis, the minor radius and the poloidal field component perpendicular to the path of integration respectively. Surfaces of constant ψ are generated from the magnetic field data measured at 90 spatial points on a 2 cm by 2 cm grid (fig. 7a). Within any six point rectangular grid area, or r.g.a. (same figure), the vertical and horizontal poloidal magnetic field components are fit to a polynomial of the form

$$B(x_i,y_i) \sim A^i y_i^2 + B^i x_i y_i + C^i x_i + D^i y_i + E^i \tag{2.2}$$

where A^i, B^i,....., E^i are the coefficients for the ith r.g.a. $B(x_i,y_i)$ is either the first or second component, vertical or horizontal, of the magnetic field at the local coordinates (x_i,y_i) within the ith r.g.a. From
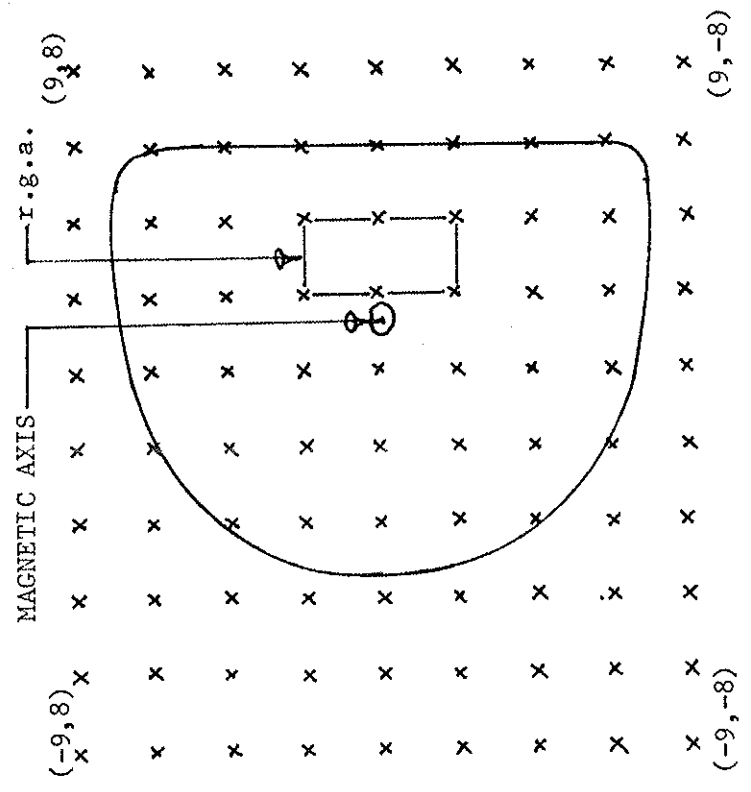
27
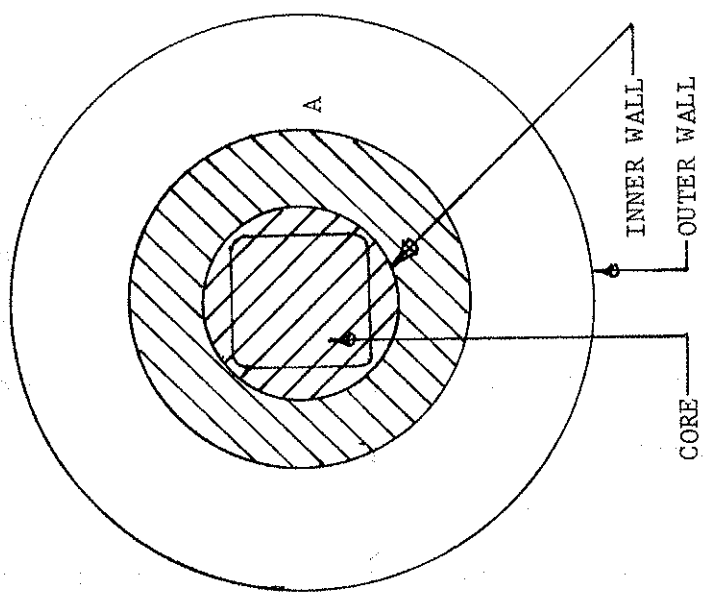
Figure 7: Experimental techniques. a) Data grid (2 cm. spacing) for magnetic flux plots.
b) Top view of experimental machine.

equations (2.1) and (2.2), an explicit polynomial in x_i and y_i can be found for ψ,

$$\psi(r,\theta) = \psi^i(x_i,y_i,x_{i0},y_{i0},A^i_{1,2},B^i_{1,2},\ldots,E^i_{1,2}) + \psi^i_0$$

$$(2.3)$$

where ψ^i_0 is the value of ψ at the edge of the r.g.a. of position (x_{i0},y_{i0}) relative to the magnetic axis $(\psi(0,\theta)=0)$. The subscript 1,2 on the magnetic field coefficients refer to the vertical or horizontal components of the poloidal field. Thus, once the position of the magnetic axis is known, the approximate value of ψ along a ray out from the axis is obtained in a stepping fashion. ψ^i_0 is determined by the final value obtained in integration through the previous r.g.a. out along that ray.

The position of the magnetic axis is found numerically by first searching for the data point with minimum B^2. This point and the eight surrounding it, define two r.g.a.'s, j-1 and j. Using explicit forms for

$$\frac{\partial \psi^j}{\partial x_j} \;,\; \frac{\partial \psi^j}{\partial y_j} \;,\; \frac{\partial^2 \psi^j}{\partial x_j y_j} \;,\; \frac{\partial^2 \psi}{\partial y_j^2} \;,\; \ldots \qquad (2.4)$$

the first order Taylor series expansion for ψ^j is

iterated to find $\nabla\psi = 0$. Five iterations are usually sufficient for convergence.

After the magnetic axis is found, the program generates an array $\psi_{sav}(k)$ containing the value of flux every 4 mm along a horizontal ray from the axis to the edge of the data grid. Then, every 5 degrees around the axis, the program searches for the radius at which $\psi(r(k,\theta)) = \psi_{sav}(k)$. These values of $r(k,\theta)$ define a flux surface.

Once the locus of points defining a flux surface is determined, various line integrals over the flux contours are approximated using Newton's 3/8 rule. The safety factor $q(k)$, toroidal current $I(k)$ and area $A(k)$ within the kth closed flux surface are given by

$$q(k) = \frac{1}{2\pi} \int_{\{r(k,\theta),\theta\}} \frac{rB_\phi}{RB\theta} \, d\theta$$

$$I(k) = \frac{1}{\mu_0} \int_{\{r(k,\theta),\theta\}} B_\theta r \, d\theta$$

$$A(k) = \int_{\{r(k,\theta),\theta\}} r^2 \, d\theta \tag{2.5}$$

The last step is to compute the toroidal current

density averaged over the annulus between two flux
surfaces,

$$J(k)=[I(k+1)-I(k)]/[A(k+1)-A(k)] \qquad (2.6)$$

Another diagnostic that is important to this study
is the electric field probe. This consists of a few turn
coil of wire 4 mm wide by 50 cm in length. As in the
case of the $\dot{B}$ probe, the coil is contained in a 1/4 inch
probe tube. The principle by which it works is
illustrated in figure 7b. The output is proportional to
the time derivative of the poloidal magnetic flux through
the coil. Assuming the poloidal field to be sinusoidal
in time, then the probe signal is a measure of the flux
between the toroidal circle A, that its tip defines, and
the machine wall. Let us designate this flux ϕ_{probe} (see
fig. 7b). The toroidal electric field at A, though, is
proportional to the amount of flux between it and the
core $= (\phi_{probe} - \phi_{wall})$. The flux linked by the wall,
ϕ_{wall}, is opposite in direction. Converting this formula
to measurable voltages we see

$$V_{loop} = V_{probe} - V_{pg} \qquad (2.7)$$

where V_{pg} is the poloidal gap voltage ($\propto \phi_{wall}$), and $V_{probe} \propto \phi_{probe}$. In actual use, care must be taken to insert the probe only on the midcylinder so that there is no component of toroidal electric field along the long sections of the coil. For the same reason the other end of the coil must be outside the machine.

C. Previous Experimental Work

Experiments heretofore performed on noncircular tokamaks have included doublets[27], ellipses[14,16] and dee's[14,16,17]. Verification of the shapes studied has occurred through external means. For example, in TOSCA[14,16], external magnetic field signals were compared with a computer model's predictions for those signals. Another variation, used on doublets and TOSCA, is the use of measured winding currents combined with appropriate plasma parameters to model the plasma. The existence of certain poloidal modes of the tearing instability has also proved to be useful in determining q, which thru the assumption of ellipticity, in turn determines the plasma shape[28]

Although existence of these equilibria has been shown in only a few papers, the stability of shapes to axisymmetric modes is even less documented. Both Toyama[17] and Bhatnagar[29] have verified the instability's existence in their respective machines, but that is the extent of their study. Bhatnagar considered the instability as a problem to be controlled, not studied. He found that the discharge length could be doubled by proper active feedback stabilization. The only major experimental study of the axisymmetric instability, previous to the present, was performed in TOSCA.

The shape of TOSCA's different equilibria is found by comparing external experimental data with predictions of an ideal MHD calculation. The experimental input consists of plasma and winding currents in addition to a limiting wall. Plasma movement, both radial and vertical, is calculated using a model that assumes the plasma to be a current filament. The difference in magnetic field, due to plasma current only, on opposite sides of the plasma gives the relative position of a current filament between those two machine sides. Cima predicts that the filament model only leads to errors of <3 mm in predicting the magnetic axis position! Using this technique of locating the magnetic axis as a

function of time, growth rates of the instability are generated. No comment is given to explain how, and when during instability growth, the growth rate is derived. This has the added consequence of shedding no light on the instability's non-linear or linear nature.

An effort was made to compare their results with related analytic and numerical studies in the literature, which were not performed for TOSCA. The plasma equilibrium is described quantitatively by the decay index $n = -R/B_z(dB_z/dR)$ averaged over the plasma volume. This average is performed using the vacuum poloidal field of the winding currents. The averaged decay index $\bar{n}$ is found to be a monotonic function of ellipticity (e). Results indicate that there are certain $\bar{n}$, or e, parameter limits beyond which no stable equilibria exist. When the equilibrium is unstable, they find its growth rate to be proportional to the shaping currents. In other words, increasing the amount of noncircular deformation decreases plasma stability. Indications are given that T_g is increased by the presence of the passive feedback coils.

D. Relative Stability of Dee, Inverse-dee and Square Equilibria

This experiment allows comparison of various plasma shapes in one machine under similar conditions. By varying the placement of the rings, which attract the plasma, the shape of the tokamak separatrix can be changed from dee to inverse-dee (figures 8a-c). If the inner rings are moved closer together, and thus nearer the plasma, the equilibrium is positioned slightly inward in major radius producing a dee (fig. 8a). An inverse-dee (fig. 8b) is created by positioning the outer rings closer together. The intermediate case is a square plasma (fig. 8c). Previous experiments concerning noncircular tokamaks have deduced the plasma shape using external measurements such as winding currents, plasma current and edge magnetic fields, combined with computer modeling. All important data in this paper, such as flux plots, current density and electric field profiles are deduced from internal probe measurements. A description of these experimental techniques is given in the previous section (III.C).
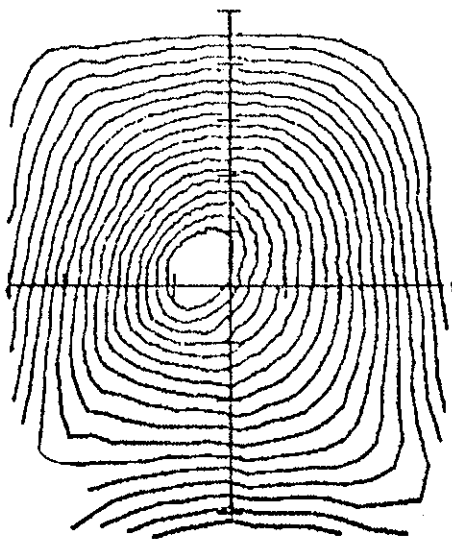
The time histories of magnetic flux plots show that the dee and inverse-dee are unstable to a non-rigid
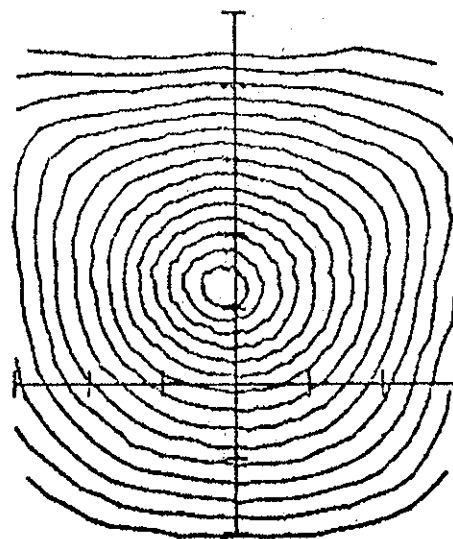
Figure 8: Experimental flux plots mapped
out with magnetic probes. Only the area
inside the separatrix is shown. Each tic
mark indicates 2 cm. a) Dee. b)
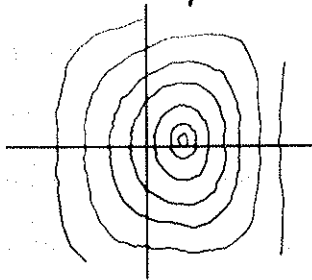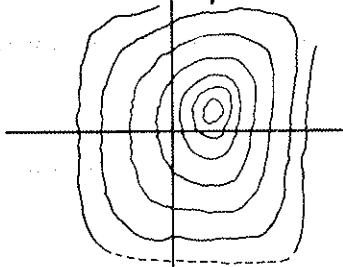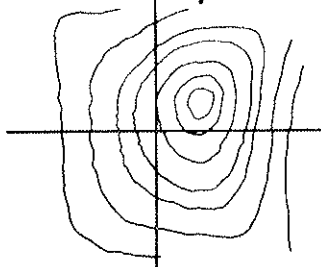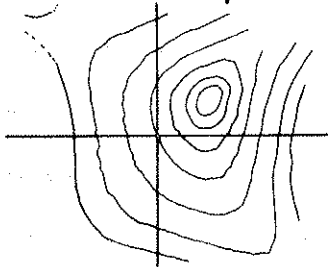Inverse-dee. c) Square.

A

B

vertical movement, along a line of sight from the
magnetic axis to a ring (figure 9). The square is stable
to this movement on the time scale of this experiment.
For the vertically unstable shapes, a plot of the
magnetic axis position, shown in figure 10, indicates
that the vertical displacement increases exponentially
with a growth time $T_g \sim 450$ usec. $T_g \sim 10^3 T_a$, where T_a is a
poloidal Alfvén time calculated with a suitably averaged
poloidal field. It is also interesting to note, and will
be discussed later, that T_g is much less than the
resistive decay time of rings and walls (15 msec) and
very close to the plasma L/R time ($\sim$ .5-2.0 msec).
Axisymmetry has been verified at several machine
azimuths. Also, the effect of plasma outside the
separatrix has been examined: That plasma was wiped out
by a movable limiter. The resulting instability growth
rate and equilibrium shape were identical to the 'normal'
case, within experimental uncertainties.

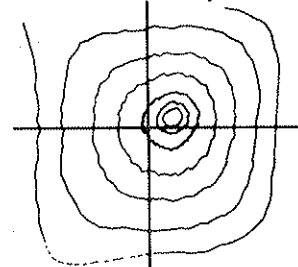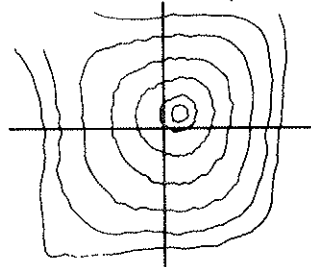We find that all these equilibria can be stabilized
to vertical movement, on the time scale of this
experiment, by precise positioning of the rings. After
the vertical movement is stabilized there still remains a
horizontal motion that is independent of the rise and
fall of the plasma current. This horizontal instability

Figure 9: Time evolution of the experimental flux plot for a) inverse-dee & b) square. The dee evolves similarly to inverse-dee.

a) Time= 1200 μ sec

b) Time=1200 μ sec

Time=1600 μ sec

Time=1600 μ sec

Time=2000 μ sec

Time =2000 μ sec

Time=2400 μ sec

Time=2400 μ sec

Time =2800 μ sec
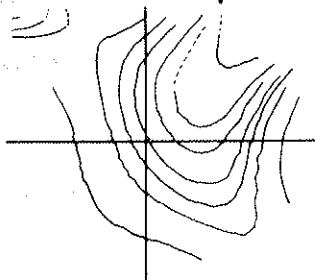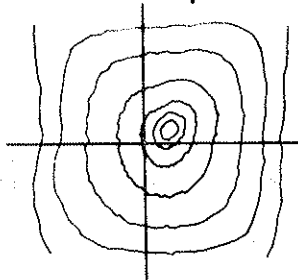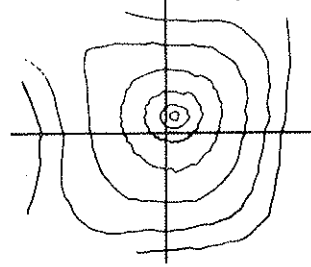
Time=2800 μ sec
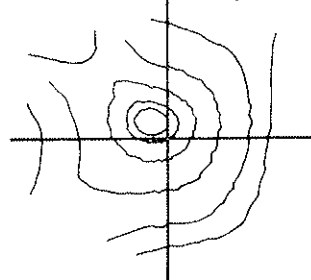
occurs in the square as well as the dee and inverse-dee.
The direction of this motion depends strictly on which
set of rings the inner plasma separatrix encircles. When
the plasma "leans" on the outer (inner) set of rings the
movement is towards increasing (decreasing) major radius.
Growth times for this horizontal instability, like the
vertical, are $^{-}10^3 T_a$. Thus a plot of the magnetic axis
position vs. time for horizontal movement is identical
to that shown for the vertical (fig. 10). This
horizontal instability does not saturate on the time
scale of the experiment.

E. Effect of Plasma Resistivity

The role of passive stabilization could be all
important to this instability and perhaps in practice
eclipse distinctions based on plasma shape. Since the
rings are inductively driven, there are no external
circuit connections between them. Thus they are free to
independently respond to the plasma motion. However, the
efficacy of passive feedback, arising from induced image
currents flowing in external conductors and plasma, is
limited by the finite resistivity of the the elements
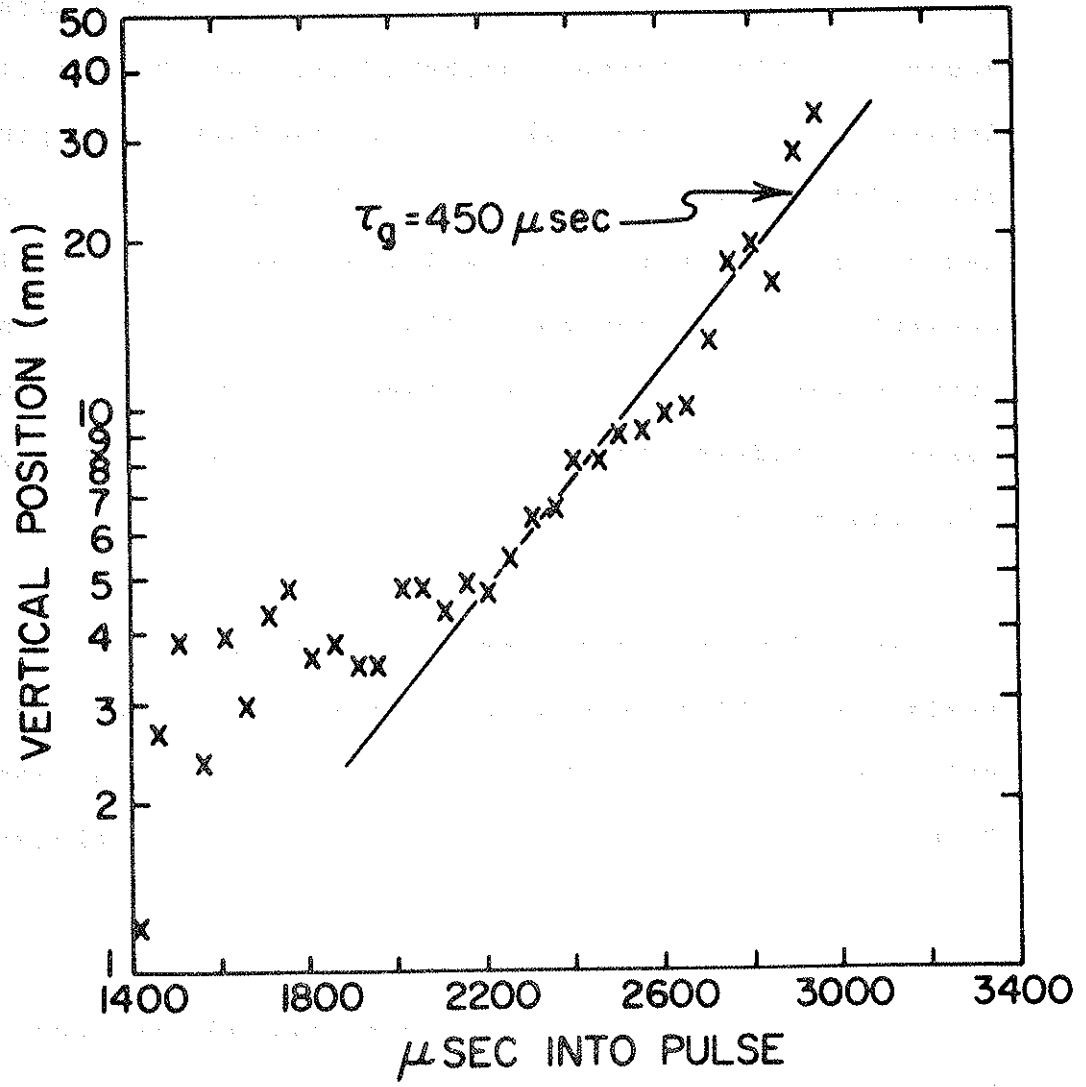
Figure 10: Distance travelled by the magnetic axis as a function of time. Uncertainty in distance travelled is 1-2 mm. 100 μsec= 500 poloidal Alfvén times.

involved. Wooton et. al.[14] found the plasma growth time of an axisymmetric instability in TOSCA to be slowed down by the resistive decay of induced stabilizing currents in the walls and external field shaping coils. The equivalent theoretical prediction has been made[8,13]. However, all these calculations assume an ideal, infinitely conducting plasma. In the Tokapole experiment the finite plasma resistivity (L/R time ~ 1 msec) is the major contributor to the damping of induced stabilizing currents. The rings and walls in this experiment have a much longer resistive decay time (15 msec.) than the plasma. Indeed, instability growth occurs on the plasma L/R time scale.

To address this issue we changed the plasma resistance while keeping the plasma inductance and shape relatively constant. Resistivity profiles are obtained from current and electric field profiles disussed in section III.C.

The resistivity profile was varied in two ways: First, by lowering the toroidal magnetic field which lowers the plasma current. Second, by puffing Ar gas, in addition to the normal H_2, to increase Z_{eff} directly. In either case the electric field profile stayed relatively

Figure 11: Spatial profiles at 2.0 msec.
a) Current density for two values of
toroidal field. The electric field
profiles for both values are similar;
only one is shown. b) Resistivity
calculated from electric field and
current in a). The separatrix is at a
minor radius of 6 cm.

Figure 12: Spatial profiles at 2.6 msec.
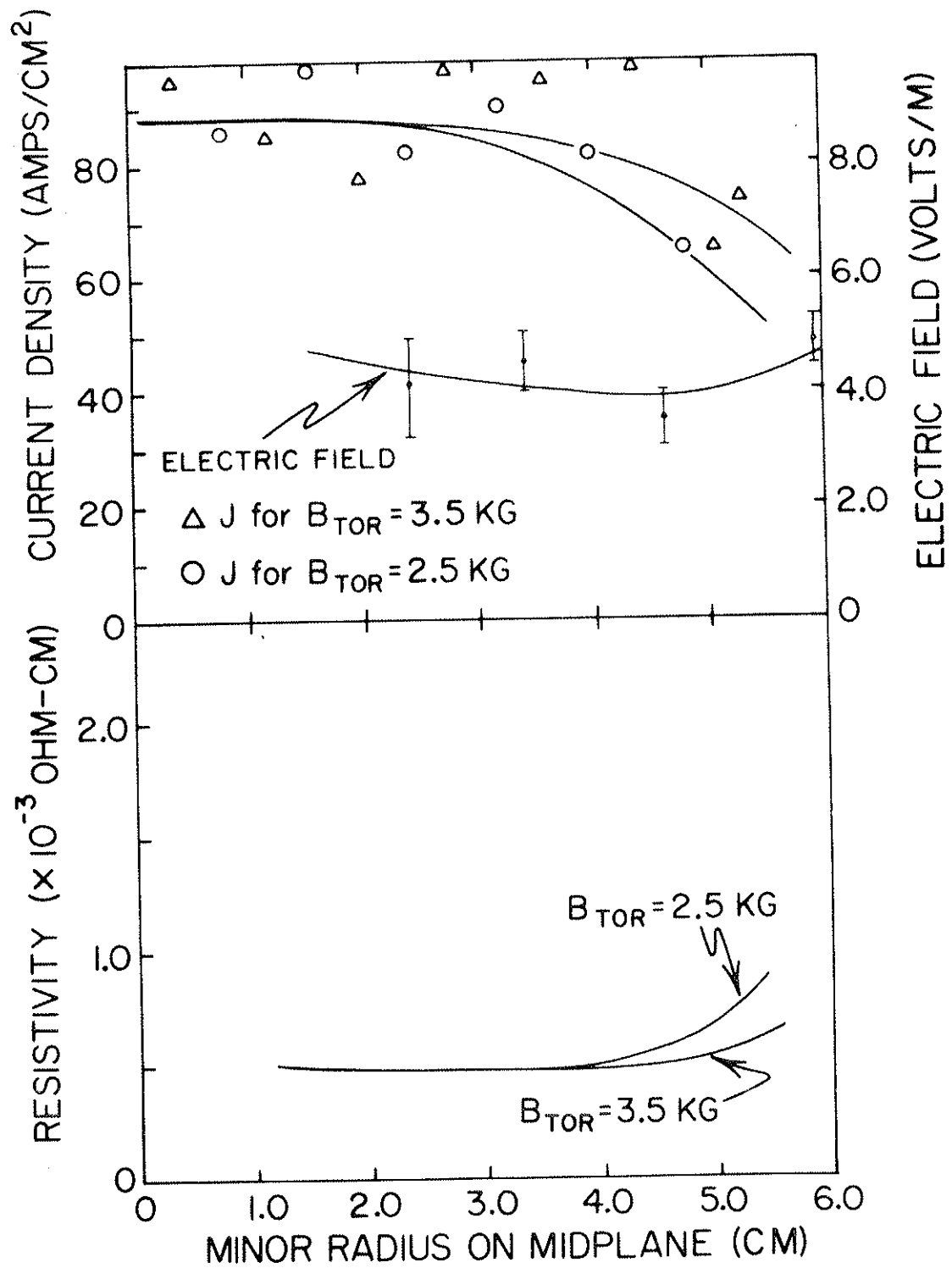a) Current density and electric fields
for two values of toroidal field. b)
Resistivity calculated from profiles in
a).
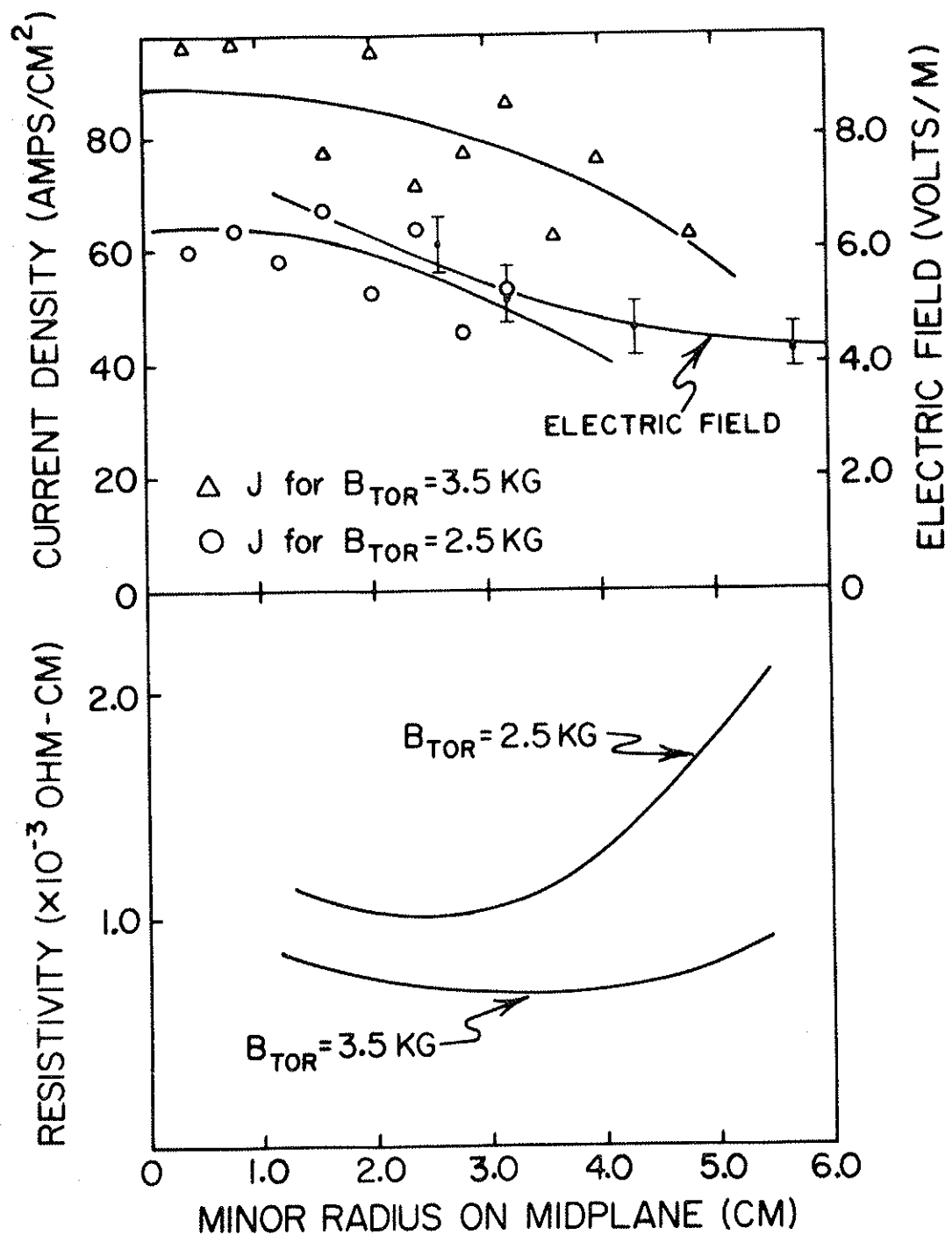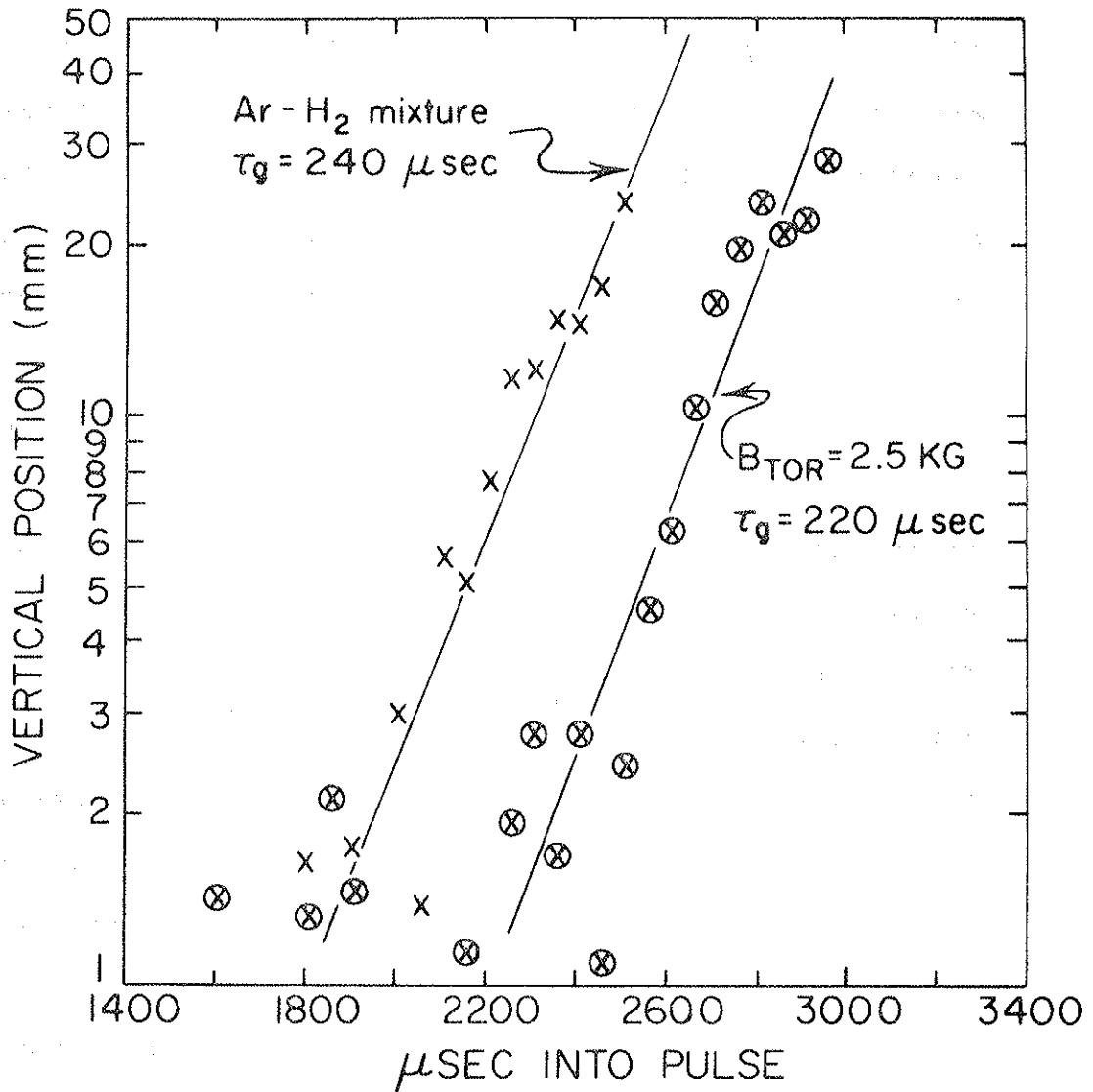
Figure 13: Distance travelled by the magnetic axis vs. time for the two methods of raising the plasma resistivity; lowering the toroidal field and puffing in Ar gas in addition to the normal H_2. Movement of the plasma in an unmodified case is shown in figure 10.

constant while the current channel width and magnitude decreased as shown for the first method in figures 11 & 12. In the particular case shown the instability onset occurred at ~ 2 msec. Such large resistance changes were necessary in order to exceed the 20% uncertainty in the measurements involved. The shape of the equilibrium was verified to be approximately the same as the unmodified case, at instability onset, by examination of the magnetic flux plots. The plasma inductance remained relatively unchanged (<10%) indicating that the decrease in the L/R time of the plasma was mainly due to the change in plasma resistance. As seen from figures 10 & 13 T_g decreased by at least a factor of 2 for either lower toroidal field or Ar puffing. Correspondingly, figure 12 indicates the plasma resistance increased by roughly a factor of two. This result is consistent with the general statement that T_g is proportional to the minimum resistive decay time in the passive stabilization circuit. In our specific case T_g is inversely proportional to the plasma resistance.

F. Effect of the Initial Plasma Position

It is important to be able to adjust the initial vertical position of the plasma in order to investigate the marginal stability case, assess the difficulty of passive stabilization and check the vertical symmetry of the machine. Through ring movement we can position the magnetic axis, initially, up to .1 minor radii above or below the midplane. We can also, for dee and inverse-dee equilibria, precisely position the plasma z-symmetrically such that it appears vertically stable.

When an otherwise unstable shape is stabilized through proper positioning, the magnetic axis exhibits an oscillatory motion (fig. 14a) about the midplane with period approximately equal to the growth time of the unstable cases. For small vertical displacements of the initial magnetic axis position from the midplane, this same oscillatory motion is superimposed upon a steady vertical movement (fig. 14b). For still larger displacements of the initial magnetic axis position, the oscillatory motion disappears and the movement is strictly exponential (fig. 10). Thus we see that increasing the initial displacement leads to faster growth. Machine vertical symmetry is verified by

Figure 14: Distance travelled by the
magnetic axis as a function of time for
different initial positions of the
inverse-dee. a) Initial position on the
midplane. b) Initial position slightly
above the midplane (3-5 mm.). When
initially positioned an equivalent amount
below the midplane identical downward
motion is observed. The case of initial
position further still above the midplane
(5-10 mm.) is shown in figure 10.

A)

B)
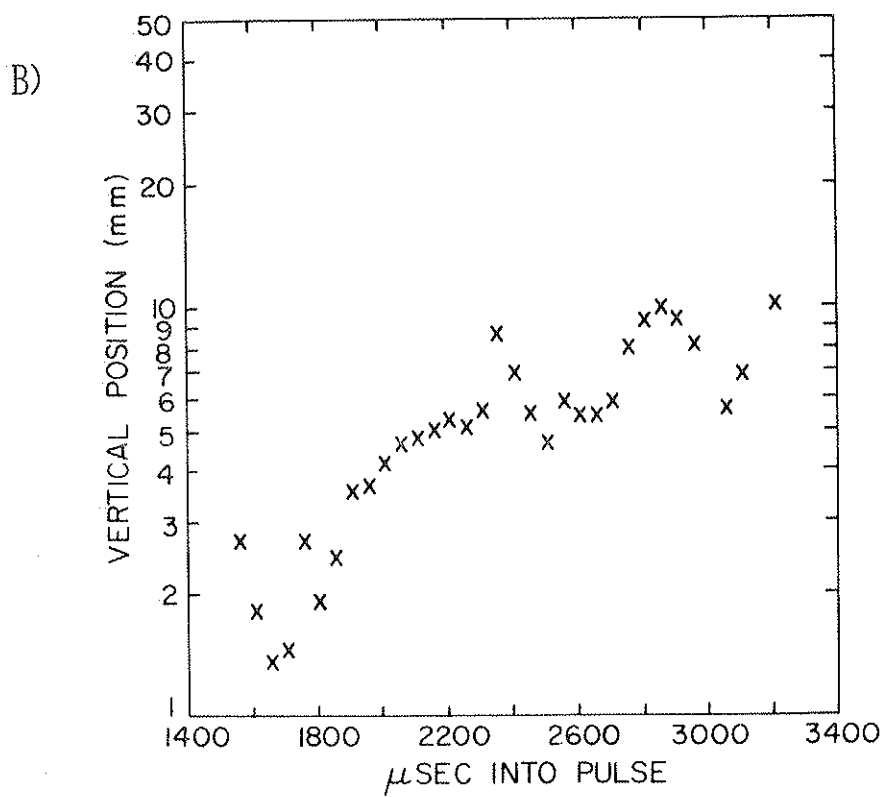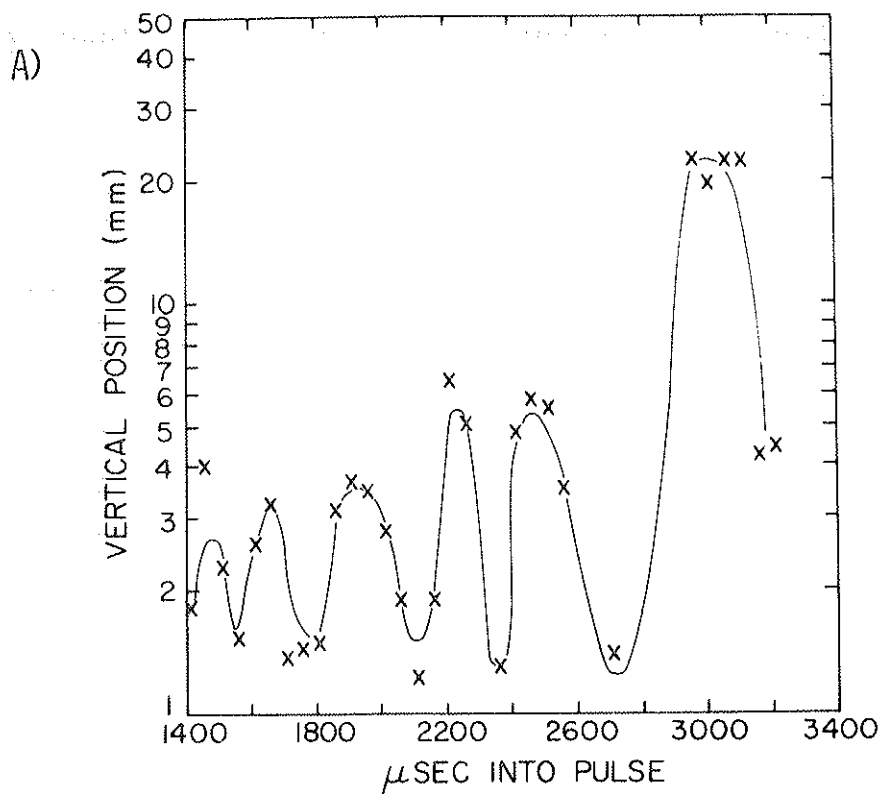
positioning the initial magnetic axis above or below the midplane and observing upward or downward motion respectively.

CHAPTER III

THEORY

A. Review of Previous Theoretical Work

To put the present study into perspective, a review
of other investigations of the axisymmetric instability
is appropriate. Quantitative comparison of the evolution
of experimental equilibria with published numerical
examples is not precise. Experimental equilibria are
poorly mirrored by analytic models (e.g. Solov'ev[30] or
Rebhan[5,6]). Also, theoretical studies have, for the most
part, defined the shape parameter limits to instability
onset as opposed to examining the relative stability of
different unstable shapes. The following is a brief
summary of the majority of the abovementioned relevant
literature.

The first person to deal with the stability to
horizontal and vertical motions of a plasma is
Yoshikawa[31]. He examines the forces on a toroidal plasma
current of minor radius a, and major radius R_0. This
examination reveals, that for horizontal stability, there

must exist a potential well such that the restoring force $(I_{tor} \times B_z)_R$ decreases slower, with major radius, than the inductive expansion force from the plasma. To express this relation we write

$$\frac{d}{dR}(2\pi R I B_z) \geq \frac{d}{dR}\{\frac{1}{2}\mu L I^2\} \qquad (3.1)$$

The same idea is applied to the restoring force in the vertical direction to give

$$(d/dz)[B_R^{ext}] < 0 \qquad (3.2)$$

These two equations are combined with the relation $(\nabla \times B_{ext})_\phi = 0$ and the assumption that $B_z \propto (R_0/R)^n$ to give

$$n \geq 0 \text{ (vertical stability)} \qquad (3.3)$$

$$n \leq 3/2 \text{ (horizontal stability)} \qquad (3.4)$$

The parameter $n = -(R/B_z)(dB_z/dR)$ is termed the vacuum field decay index. Note that it is strictly a local quantity.

A modification of Yoshikawa's result is obtained by Seki in references 7 & 8. He derives the forces acting

on the plasma current center and surface. Also taken
into account is the interaction of the plasma current
with eddy currents in a resistive shell surrounding the
plasma. The plasma is circular and a constant current
density is maintained during plasma movement. This
movement is therefore being treated as a rigid shift.
The equations of motion for the plasma are solved about
an equilibrium state using perturbation theory.
Yoshikawa's results for decay index limits are recovered
with some modification in the horizontal direction. The
presence of a wall is predicted to reduce the instability
growth rate to the inverse of a modified shell resistive
decay time.

Another study that investigates the role of decay
index in stability is Sakurai et al.[15]. An important
difference over previous work is that a tokamak with an
octupole vacuum field is studied. This, of course, leads
to noncircular equilibria. Walls are not included in
this paper. Very little information is given as to how
this calculation is performed. The criterion for
stability seems to be that if the plasma is shifted
rigidly in the vertical direction, then it is stable
given the destabilizing JxB force on it is convergent.
Reported results are that the square is vertically

stable, the dee and inverse-dee vertically unstable. Off axis equilibria were found for the dee but not for the inverse-dee.

In a departure from studies utilizing decay indices and forces, Okabayashi & Sheffield[3], using the energy principle[32], investigated plasmas characterized by ellipticity. The toroidal plasma current is modeled by a set of current filaments. A rigid vertical displacement (m=1, n=0) is given to the whole plasma column and stability is evaluated from the change in energy stored by the plasma current filaments. The two parameters m & n refer to the poloidal and toroidal mode numbers respectively. It was found that rectangular shapes are stable for $e \lesssim 3$ and ellipses for $e \lesssim 1.3$. These two were the only plasma cross sections studied. In addition, their results indicate that rectangles with flat spatial current profiles are more stable than parabolic current profiles.

Rosen[10], also studied the axisymmetric instability in the absence of external conductors. Stability of rectangular and elliptic cross sections to m=1 and m=3 axisymmetric modes is performed using a reduced form of the energy principle[33]. He finds the ellipse unstable to

a rigid shift in the direction of elongation with ellipticity limits similar to those found by Okabayashi[11]. The square was found always stable to this rigid (m=1) shift. Although the square is attracted toward the x-points, it is repeled by the antiparallel shaping currents (on the midplane and midcylinder) 45 degrees between the x-points. Thus the square would be stable to a shift but becomes unstable when an m=3 wrinkle is added to the perturbation.

A study that includes the entire energy principle applied to rigid shifts is that of Rebhan[4]. His goal is to define the analytic stability limits of noncircular deformations to dee, elliptical and inverse-dee shaped plasmas. The general form of rigid movement is utilized which includes flipping as well as linear motion. Other assumptions made in this paper include the absence of external conductors, incompressible plasma motion, and $p'(\psi)$ and $I'(\psi)$ being constants. I and p are RB_{tor} and plasma pressure, respectively. After writing down a form of the energy principle, Rebhan points out that the plasma term

$$\frac{1}{2}\int_S (\underline{\xi} \cdot \underline{\nabla} p^*) \, \underline{\xi} \cdot d\underline{S} \qquad (3.5)$$

drives the vertical instability. $\underline{\xi}$ is the perturbation, p^* is the total pressure ($p+B^2/2$) and S is the surface of the plasma. In other words, a gradient of the total pressure drives the instability. A stabilizing influence is due to flux compression in the vacuum through the term

$$\frac{1}{2}\int_S (\underline{B}\cdot\delta\underline{B}_v)\ \underline{\xi}\cdot\underline{dS} \qquad (3.6)$$

Rebhan's results indicate, for rigid vertical movements, that the ellipticity limit for total stability is lower for ellipses than for dee or inverse-dee shapes. In studying his equations, one finds that all toroidal field terms are absent. This occurs because he is modeling a purely vertical shift, which does not stretch the toroidal field. He interprets this as the plasma slipping through the toroidal field.

Rebhan & Salat[5] extend this work in Rebhan's second axisymmetric instability paper by including rectangles among the shapes studied. They drop Solov'ev equilibria in favor of a constant pressure, surface current model that allows for non-rigid as well as rigid shifts. The shapes studied are described by

$$\frac{e^2}{A^2} = e^2(R-1)^2+(1+T_3^2)z^2-2AT_3(R-1)z^2-T_4A^2(R-1)^2z^2 \qquad (3.7)$$

where e, T_3 and T_4, are shape parameters describing ellipticity, triangularity and rectangularity respectively. Also, A, R and z are the aspect ratio, major radius and vertical distance above the midplane. The aim of this work is to again define parameter limits, but in this case, with a different set of parameters and for nonrigid movements. Qualitatively, what is found is that squares and ellipses have approximately the same ellipticity limit for total stability. But, in contrast to rigid shifts, increasing T_3 (deeness) implies a lower ellipticity limit. Also, a typical dee or inverse-dee $(|T_3| \sim .3)$ has a lower ellipticity limit than a typical square $(T_4 \sim .3)$. In studying the form of the non-rigid movement, we see that the perturbation is largest where the surface poloidal curvature is greatest (near the x-point). Rebhan & Salat predict that in the presence of a conducting wall this instability will have a lower growth rate.

A paper, similar in nature to those mentioned of Rebhan's, is that by Chu & Miller[34]. Here the energy principle is minimized numerically with respect to arbitrary displacements. An improvement, however, is the allowance of a nonuniform plasma current. They find that the minimizing displacement, or most unstable eigenmode,

for rectangles and dee's always contains a nonnegligible triangular component (m=3). This result, that the unstable displacement is nonrigid, agrees well with Rebhan[5] and Rosen[10]. Wall stabilization was included in Chu & Miller's work and found necessary for elliptical plasmas. Peaked current profiles were found to be less stable than flat profiles in the presence of a wall. Rectangular shapes, overall, were more stable than ellipses.

Using numerical equilibria, Becker & Lackner[12] computed the asixymmetric stability of dee's and squares using a similar method to that of PEST[20], which is described in section III.C. However, the inverse-dee is not studied nor are external conductors included in this model. Squares are found to be more stable to non-rigid vertical movements than the dee. Additionally, peaked current profiles are predicted to be more stable than flat. This result is different from the previous paper for reasons that are undecipherable from these reports.

In the continuing improvement of these studies, and computer codes in general, Jardin[13] pushes on into the nonlinear regime. The code he used is described in detail in section III.D, but it will briefly be described

here for completeness. This code, PATENT[13,23], steps the full 2-D time dependent MHD equations in time using a flux coordinate system which gives us a continuous picture of the plasma shape. Current carrying coils in the vacuum can be allowed to interact with the plasma and themselves through circuit equations. The square is found to be more stable than the dee or inverse-dee. In the presence of passive stabilization, the square and other equilibria of small deeness can be stabilized on the time scale of his code (200 toroidal Alfvén times). In addition, in a statement similar to Rebhan's, Jardin reports that the portion of plasma nearest the current carrying coils deforms the most.

Using the linear stability code ERATO[35] and analytic Solov'ev equilibria, Bernard et al.[9] study axisymmetric stability as a function of parameters used by the first Rebhan paper[4]. The difference between these papers is that here allowance is made for non-rigid displacements. Qualitatively, agreement is reached with previous work in that the unstable deformation is found to be greatest near x-points. Also, walls are stabilizing, thus increasing the ellipticity limits of a given triangularity. Bernard joins Jardin[13] in comparing the relative stability of unstable equilibria: the dee is

more stable than the inverse-dee. Critical distances to the wall for stabilization are quoted as a function of ellipticity and triangularity.

Rebhan & Salat[6] further extend their work by including passive and active feedback due to external conductors. The new terms added to the energy principle are for active feedback

$$\delta W_j = \frac{1}{2} \int_S (\underline{B}_v \cdot \underline{\delta B}_1) \ \underline{\xi} \cdot \underline{dS} \tag{3.8}$$

and passive feedback

$$\delta W_p = \frac{1}{2} \int_S (\underline{B}_v \cdot \underline{\delta B}_2) \ \underline{\xi} \cdot \underline{dS} \tag{3.9}$$

where $\underline{B}_v$ is the total vacuum field. $\underline{\nabla} \times \underline{\delta B}_1$ and $\underline{\nabla} \times \underline{\delta B}_2$ are the currents in the active and passive feedback coils respectively. δW_p is always positive, or stabilizing, for quasi-static field changes. Therefore, that term can be dropped retaining a sufficient stability condition

$$\delta W_0 + \delta W_j \geq 0 \tag{3.10}$$

where δW_0 is the perturbed energy without feedback (see Rebhan[5]). Feedback for properly positioned z-symmetric

coils is found possible for dee, inverse-dee, square and elliptical cross sections. If the elongation is too large, i.e. a belt pinch, feedback stabilization becomes more difficult. For smaller elongations, feedback coils in the direction of the x-points are always effective.

Summary

Although the visualization of the axisymmetric instability is simple, the modeling of its action and character is not. As can be seen by reading the above review, the degree of complexity and accuracy of these studies has increased over time in search for the most physical model. Starting with a simple current filament, generalization was made to current profiles and the linearized forces acting upon them. Noncircular shapes were then included and the treatment modified to linearization of the MHD equations, the energy principle. Finally, allowance has been made for the stabilization due to external conductors and an investigation using the full set of nonlinear MHD equations was performed. It is easy to see that the latest papers present the most accurate modeling process but the question arises as to which is the most physical. The most important difference between the latter studies is the type of

equilibria utilized: analytic or numerical. Certainly numerically generated equilibria are more useful because of their ability to represent almost any shape and set of plasma parameters. Inclusion of feedback is definitely important because many shapes of interest are axisymmetrically unstable.

B. Numerical Equilibrium Code

The reasons for undertaking a theoretical study to complement this experiment are twofold. First, previous theoretical work, for the most part, has emphasized defining limits in parameter space to absolute stability. For the Tokapole and other noncircular tokamaks, most realizable and interesting equilibria are unstable to axisymmetric modes. Therefore, what becomes of greater interest than stability limits, is the relative stability of these equilibria with an eye toward the use of stabilization; either passive or active. Besides the redirection of theoretical emphasis, the second reason for this study is that published work does not accurately reflect our experimental machine.

To perform a stability calculation on an equilibrium that closely parallels the physical reality of the Tokapole, the Princeton Equilibrium program[20] was modified by Dr. Alan Todd to include the Tokapole walls. In this section, I will describe the equilibrium program which was originally written by Dr. S.C. Jardin, and the Grad-Shafranov equation which it utilizes. In sections III.C and D, the PEST and PATENT stability codes will be described. These both utilize the numerical equilibrium, that will be described in this section, as input. Theoretical predictions by these stability codes will be described in sections III.E and F.

Basic to this discussion of numerical equilibria is the Grad-Shafranov equation. The usual cylindrical coordinates are used here (R,ϕ,z) with the z axis being the major or symmetry axis of the toroid (fig.15a). Keeping in mind that ϕ, the toroidal angle, is an ignorable coordinate, we can write down the magnetic field

$$\underline{B} = \underline{\nabla} \times (A_\phi \hat{\phi}) + B_\phi \hat{\phi} \qquad (3.11)$$

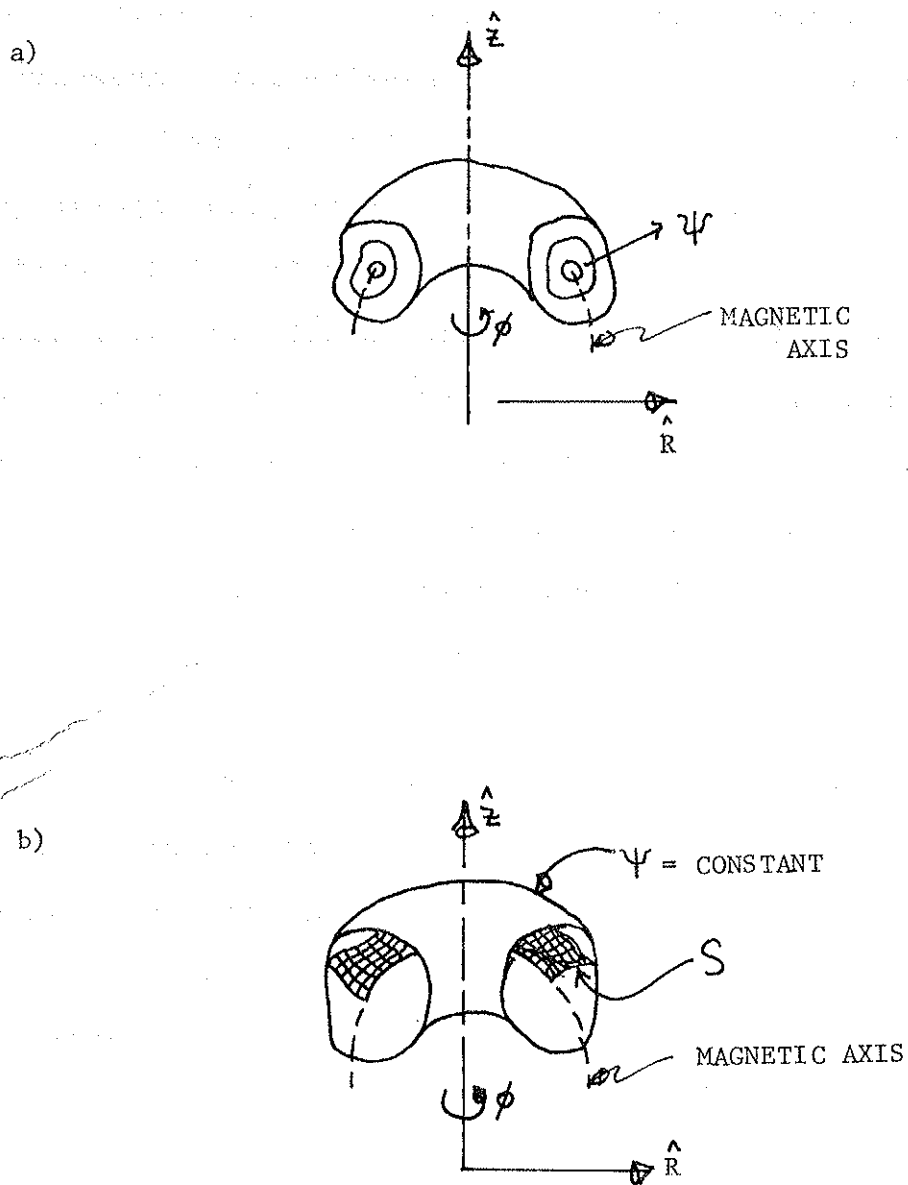Following the lead of other derivations, we now introduce a stream function ψ

Figure 15: Description of the numerical equilibrium code. a) Cylin-
drical coordinate system used. Note nested flux surfaces. b) Surface
S over which poloidal flux, ψ, is integrated.

$$\underline{B} = \underline{\nabla}\times(\ \underline{\nabla}\phi) + RB_\phi\underline{\nabla}\phi$$

$$= \underline{\nabla}\psi\times\underline{\nabla}\phi + B_\phi\hat{\phi}$$

$$= \frac{1}{R}\frac{\partial\psi}{\partial z}\hat{R} - \frac{1}{R}\frac{\partial\psi}{\partial R}\hat{z} + B_\phi\hat{\phi} \qquad (3.12)$$

It can be shown that ψ is proportional to the poloidal flux

$$\psi = \psi_{pol}/2 = (1/2\pi)\int_S \underline{B}_{pol}\cdot\underline{dS} \qquad (3.13)$$

by evaluating the above integral using 3.12. The surface S (fig. 15b) is toroidal with one edge on a fixed circle, the other intersecting a point whose poloidal flux is to be measured. Contours of constant ψ form nested surfaces within the plasma.

The current density J is computed from

$$\mu_0\underline{J} = \underline{\nabla}\times\underline{B}$$

$$= \frac{1}{R}[\hat{z}\ \frac{\partial}{\partial R}(RB_\phi) - \hat{R}\frac{\partial}{\partial z}(RB_\phi)]$$
$$-\frac{1}{R}[R\frac{\partial}{\partial R}\ \frac{1}{R}\ \frac{\partial\psi}{\partial R} + \frac{\partial^2\psi}{\partial z^2}]\hat{\phi}$$

$$= -(\Delta^*\psi/R)\hat{\phi} + \underline{\nabla}(RB_\phi)\times\underline{\nabla}\phi \qquad (3.14)$$

68

where B_ϕ is the toroidal field magnitude, and we define the operator

$$\Delta^* \psi \equiv R\frac{\partial}{\partial R} \frac{1}{R} \frac{\partial \psi}{\partial R} + \frac{\partial^2 \psi}{\partial z^2} \tag{3.15}$$

Using 3.12 we see that $\underline{B} \cdot \underline{\nabla}\psi = 0$, indicating that $\underline{B}$ lies on a flux surface. From this we can show that the pressure p is a surface quantity $(p = p(\psi))$ by $\underline{B} \cdot \underline{\nabla}p = \underline{B} \cdot (\underline{J} \times \underline{B}) = 0$. Solving for p we see

$$\mu_0 p'(\psi)\underline{\nabla}\psi = [-(\Delta^*\psi)\underline{\nabla}\phi + \underline{\nabla}(RB_\phi) \times \underline{\nabla}\phi] \times$$
$$[\underline{\nabla}\psi \times \underline{\nabla}\phi + B_\phi R\underline{\nabla}\phi]$$

$$= -\frac{\Delta^*\psi}{R^2} - \frac{B_\phi R \underline{\nabla}(RB_\phi)}{R^2} \tag{3.16}$$

RB_ϕ must also be a surface quantity because, like all other terms in this equation, $\underline{\nabla}(RB_\phi)$ must be parallel to $\underline{\nabla}\psi$. Thus we define

$$I(\psi) \equiv RB_\phi \tag{3.17}$$

$I(\psi)$ is proportional to the poloidal current inside a flux surface characterized by ψ. This can be shown using the representation for $J(\psi)$ from 3.14

$$I_{pol} = \int \underline{J}_{pol} \cdot d\underline{S}$$

$$= \int [\frac{\nabla(B_\phi R)}{\mu_0 R} \times \hat{\phi}] \cdot d\underline{S}$$

$$= \int \frac{I'(\psi) 2\pi R d\psi}{\mu_0 R} = I(\psi)\frac{2\pi}{\mu_0}$$

i.e. $I(\psi) = \frac{\mu_0}{2\pi} I_{pol}(\psi)$ $\qquad\qquad$ (3.18)

Using 3.14 & 3.15 we can rewrite the force balance equation, 3.16, as

$$-\Delta^* \psi = R^2 \mu_0 p'(\psi) + II'(\psi) = \mu_0 R J_{tor}(\psi) \qquad (3.19)$$

which is the Grad-Shafranov equation. Jardin, for use in his equilibrium code, renormalizes 3.19 and changes units to obtain

$$\Delta^* \psi = -(2\pi/B_0)^2 R^2 p'(\psi) - (2\pi x_0)^2 gg'(\psi) \qquad (3.20)$$

where x_0 is the major radius at which the constant B_0, the toroidal field magnitude, is specified.

To solve equation 3.20, which is an elliptic equation, two things must be specified. 1) ψ on the boundary (real space) and, 2) the right-hand side (RHS)

of the equation, RJ_{tor}, everywhere. However, since RJ_{tor} must be specified as a function of (ψ, R) and we do not know, a priori, how ψ depends on real coordinates, a double nest of iterations is used. The inner loop solves for the RHS, given ψ on the boundary and a specified form for $g(\psi)$ and $p'(\psi)$. The outer loop calculates a new ψ on the boundary given the RHS. The inner loop is made to converge before the outer loop is accessed. The equilibrium is found when both loops converge.

The iterations are performed usng a rectangular finite difference grid, whose spacing, Δx and Δz, is specified. Other parameters that need to be specified are the value for the total toroidal plasma current, the position of, and current in, each external current, the toroidal field B_0 at a particular major radius x_0, the grid size and the functional form for $RJ_{tor}(\psi)$. This form is generated by the two functions $p(\psi)$ and $g(\psi)$ where

$$g(\psi) \equiv 1 - g_p \hat{g}(\psi) \qquad (3.21)$$

The parameter g_p is used to maintain the total plasma current constant during iterations. Explicitly

$$\hat{g}(\psi) = ([\psi_{lim} - \psi]/[\psi_{lim} - \psi_{min}]) \quad ,$$

$$p(\psi) = ([\psi_{lim} - \psi]/[\psi_{lim} - \psi_{min}]) \qquad (3.22)$$

where ψ_{lim} and ψ_{min} are the values of ψ at the limiter and magnetic axis, respectively. Also specified are p_0, α and β, parameters which describe the toroidal current profile. For α, β on the order of 1 a flat current profile is produced similar to that of the Tokapole. For α, β on the order of 2, a parabolic profile is produced similar to most other tokamaks.

C. The PEST Stability Code

Much effort, in plasma theory, has been expended to determine the axisymmetric stability properties of different equilibria. There are two main classes of techniques to tackle this problem: The first, and most obvious, is to perturb the plasma and watch its time development. This technique has been implemented in the form of the PATENT code described in the following section (III.D.). It has the advantage of providing

insight into the nonlinear aspects of the instability growth. What will be discussed in this section is the second technique which can be termed a 'variational' approach. All versions of this technique have their basis in the energy principle as stated by Bernstein et al.[32]. If knowledge of stability only, yes or no, is desired, not growth rates, then the perturbed potential energy

$$\delta W = -(1/2) \int dV (\underline{\xi} \cdot \underline{F}(\underline{\xi}) \qquad (3.23)$$

is studied. $F(\xi)$ is the perturbed force which is a function of the perturbation ξ. Should any perturbation cause $\delta W < 0$, then the kinetic energy is correspondingly increased indicating the system is unstable.

If in addition to knowledge of stability, growth rates are desired, then inclusion of a kinetic energy term will supply time derivatives. Equivalence of Hamilton's principle applied to the system Lagrangian has been shown[36]. In the literature, the application of this principle is referred to as making the Lagrangian L stationary

$$\delta \int L \, dt = \delta \int dt [K.E. - W(\xi,\xi)] = 0 \qquad (3.24)$$

where L is of the form

$$L = \int dV \; (\tfrac{1}{2}\rho v^2 - \frac{P}{\gamma - 1} - \frac{B^2}{2u_0})$$

(3.25)

All the terms above are clear as to their origin and are written in terms of the perturbation $\underline{\xi}$ by linearizing the MHD equations:

$$\rho \frac{\partial v}{\partial t} = -\underline{\nabla} p + \underline{J} \times \underline{B}$$

$$\underline{J} = \frac{1}{u} \underline{\nabla} \times \underline{B}$$

$$\frac{\partial B}{\partial t} = -\underline{\nabla} \times \underline{E}$$

$$\underline{E} = \underline{v} \times \underline{B}$$

$$\frac{\partial p}{\partial t} = \underline{v} \cdot \underline{\nabla} p - \gamma p \underline{\nabla} \cdot \underline{v}$$

$$\frac{\partial \rho}{\partial t} = -\underline{v} \cdot \underline{\nabla} \rho - \rho \underline{\nabla} \cdot \underline{v}$$

(3.26)

The terms presented in 3.25 are all that is needed to evaluate stability with respect to kink and interchange modes for normal tokamak geometry. However, in the presence of external conductors, more terms should be added. Dewar[21] does this by including the 'kinetic'

energy of the currents involved through a $1/2LI^2$ term. Todd[22] has implemented this new term in the modified PEST code used here.

In practice, the energy terms must be written as a function of some general perturbation $\underline{\xi}$. In the case of the PEST code it appears that $\underline{\xi}$ is presented as the sum of toroidal harmonics u^n_{k+1} of order n and degree k-1/2:

$$u^n_{k+1} = \{\cosh\mu - \cos\eta\}^{1/2} e^{i(n\phi+k\eta)} P^n_{k-1/2}(\mu) \qquad (3.27)$$

These harmonics are centered at various axes in the plasma, to model the plasma shape and current, and at each of the external current sources with accompanying image. The symbols μ, η and ϕ represent the toroidal coordinates centered at these axes. Each potential energy term is minimized with respect to the coefficients of these toroidal harmonics. When the most unstable $\underline{\xi}$ is found, the kinetic energy is evaluated. Because this calculation is linearized, $K(\underline{\xi},\underline{\xi})$, the kinetic energy can be written as $w^2 K(\underline{\xi},\underline{\xi})$ so 3.24 becomes

$$w^2 = \frac{W(\underline{\xi},\underline{\xi})}{K(\underline{\xi},\underline{\xi})} \qquad (3.28)$$

and a growth rate can be solved for. The notation $W(\xi,\xi)$

is used in the literature to denote that W is quadratic in ξ. The eigenmode in toroidal coordinates is decomposed into its poloidal components so that the principal poloidal mode numbers can be ascertained. Typical output showing the strength of each poloidal component and also the velocity field are shown in figure 16.

D. PATENT Code Description

Linear codes can quickly, in terms of computer time, give relevant results. Time-dependent codes, as mentioned in section III.B, can possibly provide insight into the nonlinear interaction of the modes and physical elements involved. What is meant by nonlinear and time dependent is that PATENT follows the full set of nonlinear MHD equations through time.

PATENT takes the numerical equilibrium described in Section III.B and displaces it some small amount above or below the midplane (usually .02 minor radii). If an equilibrium is unstable, then the displacement will increase with time. If the configuration is stable, the magnetic axis will oscillate about the midplane.

Figure 16: PEST predictions for an
unstable PDX equilibrium. a) Magnitude
of poloidal fourier components (ordinate)
vs. Psi (abscissa). Each curve
represents a different poloidal component
ranging from m=-15 to 15. The dominant
components, here, as for all vertical
axisymmetric modes are m=3, -3. b)
Velocity field for this perturbation.
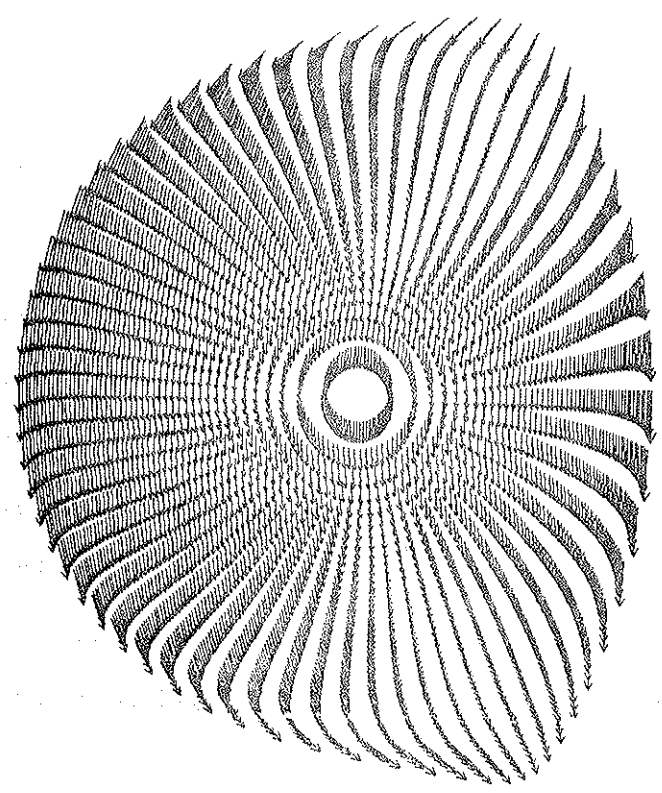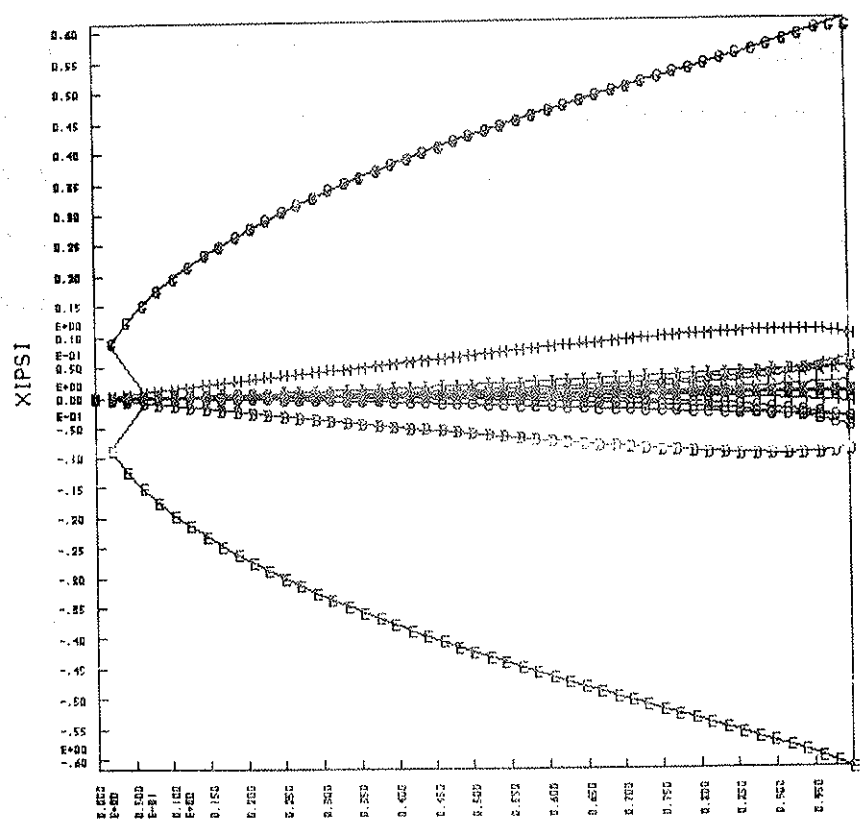
This code, like PEST, can include rings in its stability calculation. Their resistance can be varied, but this ability is of little use since the ring L/R time cannot be allowed to approach the instability growth time without numerical instability ensuing. Thus, any external conductors, as in PEST, have essentially infinite conductivity.

In both codes, these rings can be electrically arranged in almost any circuit imaginable. In the case of PATENT, the ring currents I_i are described by

$$\sum_k M_{ik}\dot{I}_k + n_i\dot{K}_i + n_i r_i I_i = n_i v_i \tag{3.29}$$

where

$$M_{ik} = -n_i n_k G(\underline{x}_i, \underline{x}_k) \tag{3.30}$$

is the mutual inductance between coils i and k. $G(\underline{x}_i, \underline{x}_k)$ is the infinite medium Green's function. K_i is the poloidal flux at coil i due to the plasma current. The plasma and external currents communicate through boundary conditions at the plasma surface and the Green's function. The number of turns, voltage and resistance of coil i are n_i, v_i and r_i respectively. Application of Kirchhoff's

law to these circuit equations leads to a set of equations describing dI_i/dt. These are stepped forward in time, as dynamical variables, along with the full set of MHD equations.

The technique applied in PATENT to solve these equations is termed the dynamical grid method. This method, described in great detail elsewhere[23], is neither Eulerian (in the moving plasma coordinate system) nor Lagrangian (in the laboratory frame), but is based on the structure of the changing magnetic field. A time-dependent nonorthogonal magnetic flux coordinate transformation is introduced to accomplish this. This transformation to the coordinates ψ, proportional to poloidal flux, and Θ, a measure in the direction around a flux surface, determines the grid used in the computation.

An important consequence of this technique is that the plasma shape can be followed through time. This is because the positions of grid points, which outline each flux surface, are treated as dynamical variables. The explanation of how the MHD equations are recast in this coordinate system as well as the two step advancement scheme is also given in reference 23.

The output capabilities of this code include flux and velocity vector plots at specified time intervals, the position of specific grid points, and the magnitude of feedback currents as a function of time. Samples of output are shown in figures 17 & 18.

E. Results Without Passive Feedback

The PEST code is used to evaluate the axisymmetric stability of a range of Tokapole and PDX equilibria (figures 19-21) from inverse dee to square to dee. Comparison of Tokapole and PDX results can be used to determine the generality of the experiment. Stability may be calculated with the rings and walls either included or excluded to assess the role of passive stabilization. The deeness of the equilibria may be described by fitting the flux surface just inside the separatrix by equation 3.7, where e is the ellipticity, T_3 is a measure of the triangularity or deeness, T_4 is a measure of rectangularity and A is the aspect ratio. This expression is useful because it allows a description of dee, inverse-dee, elliptical as well as square shaped

Figure 17: Predictions by PATENT for vertical position of the magnetic axis as a function of time. The ordinate is in units of 10^{-1} minor radii. Initial perturbation, in this case, is .02 minor radii. The abscissa is in units of toroidal Alfven times $(\mu_0 \rho a^2/B^2)^{1/2}$.
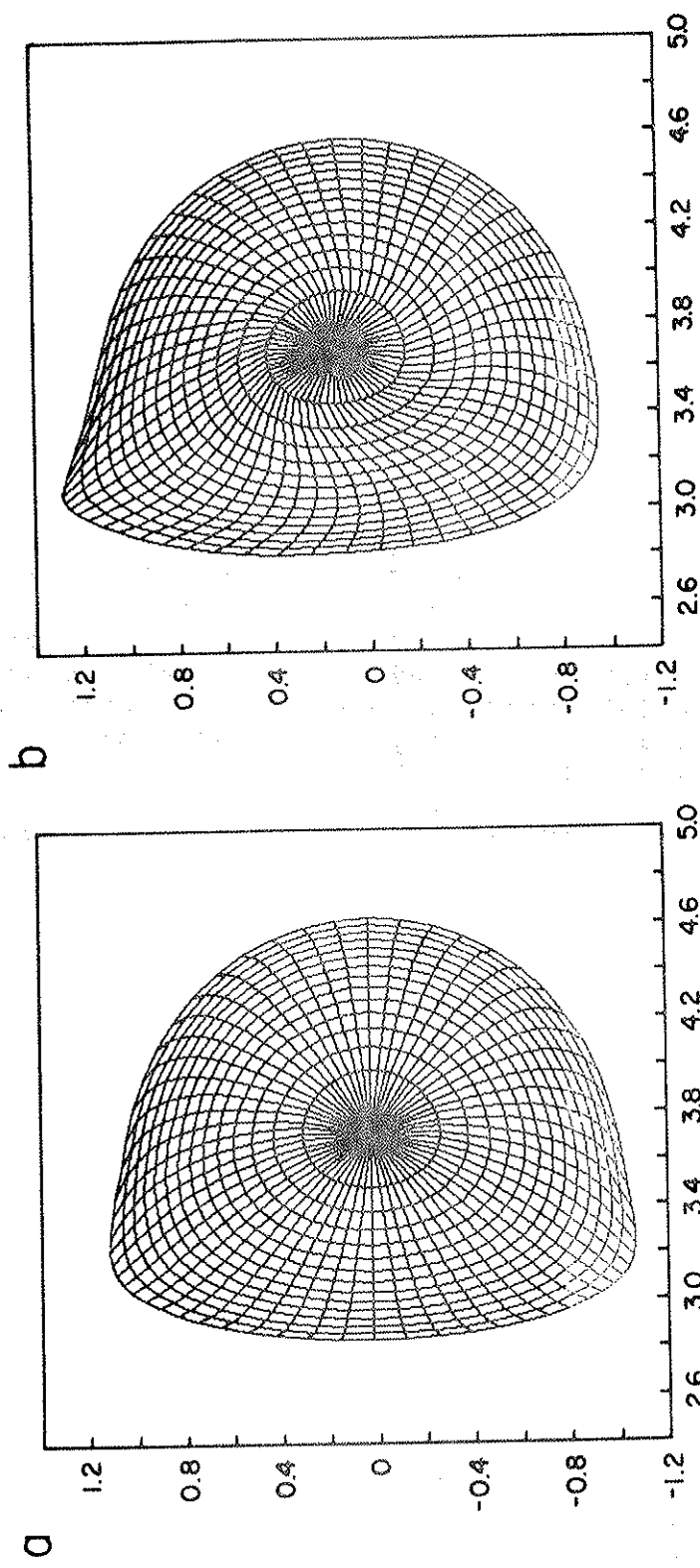
83
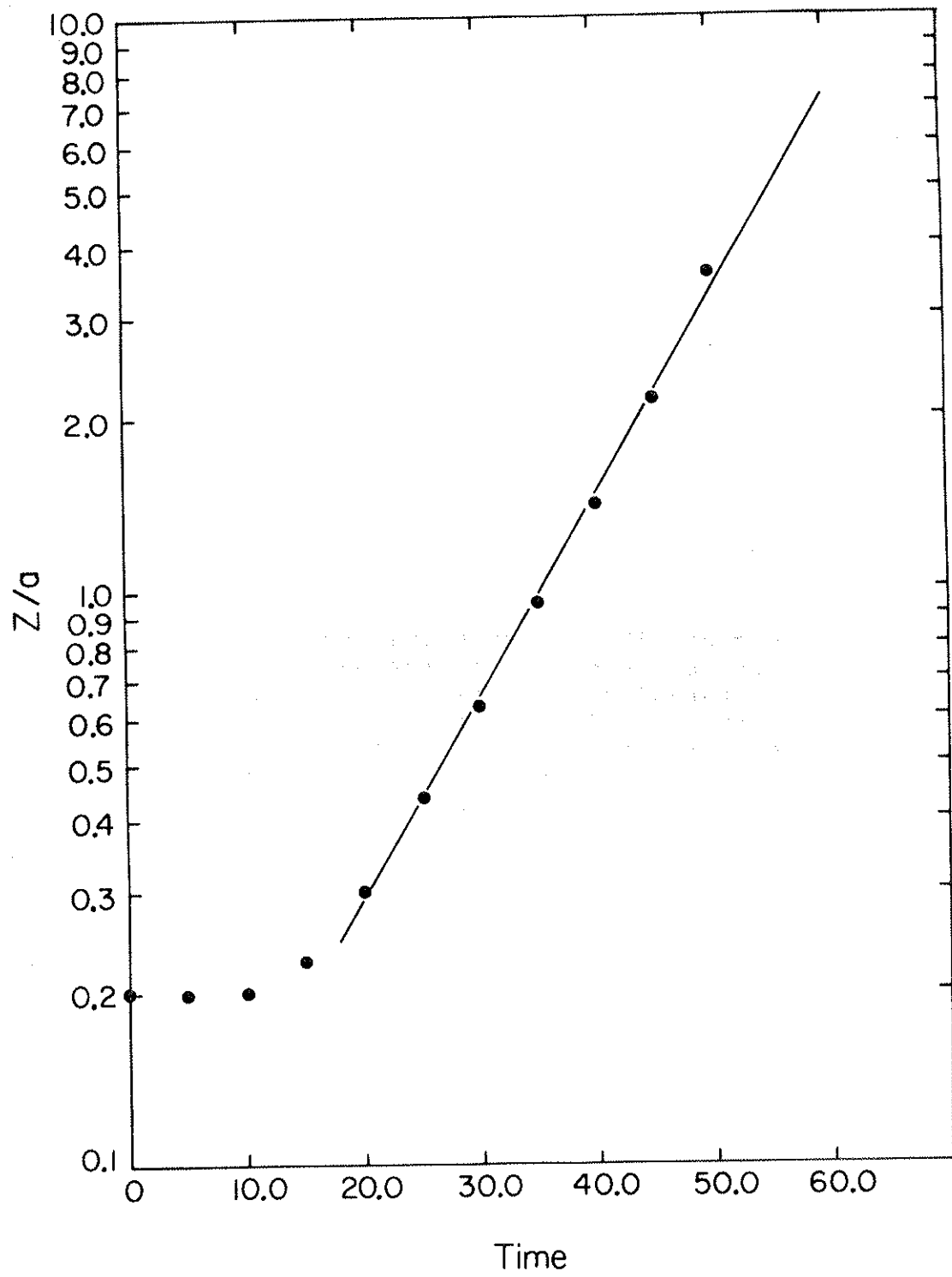
Figure 18: Theoretically predicted (PATENT) deformation of the plasma shape for PDX.
a) Initial equilibrium. b) t=100 toroidal Alfvén times.

Figure 19: Theoretical vertical growth rates vs. T_3, as predicted by PEST, for the Tokapole. Three cases are shown. X - Without passive stabilization. 0 - Only rings included. ☐ - Only walls included. Square, dee and inverse-dee shapes are described by $T_3=0$, <0 & >0 respectively. Including both rings and walls completely stabilizes all shapes other than extreme $|T_3|$.
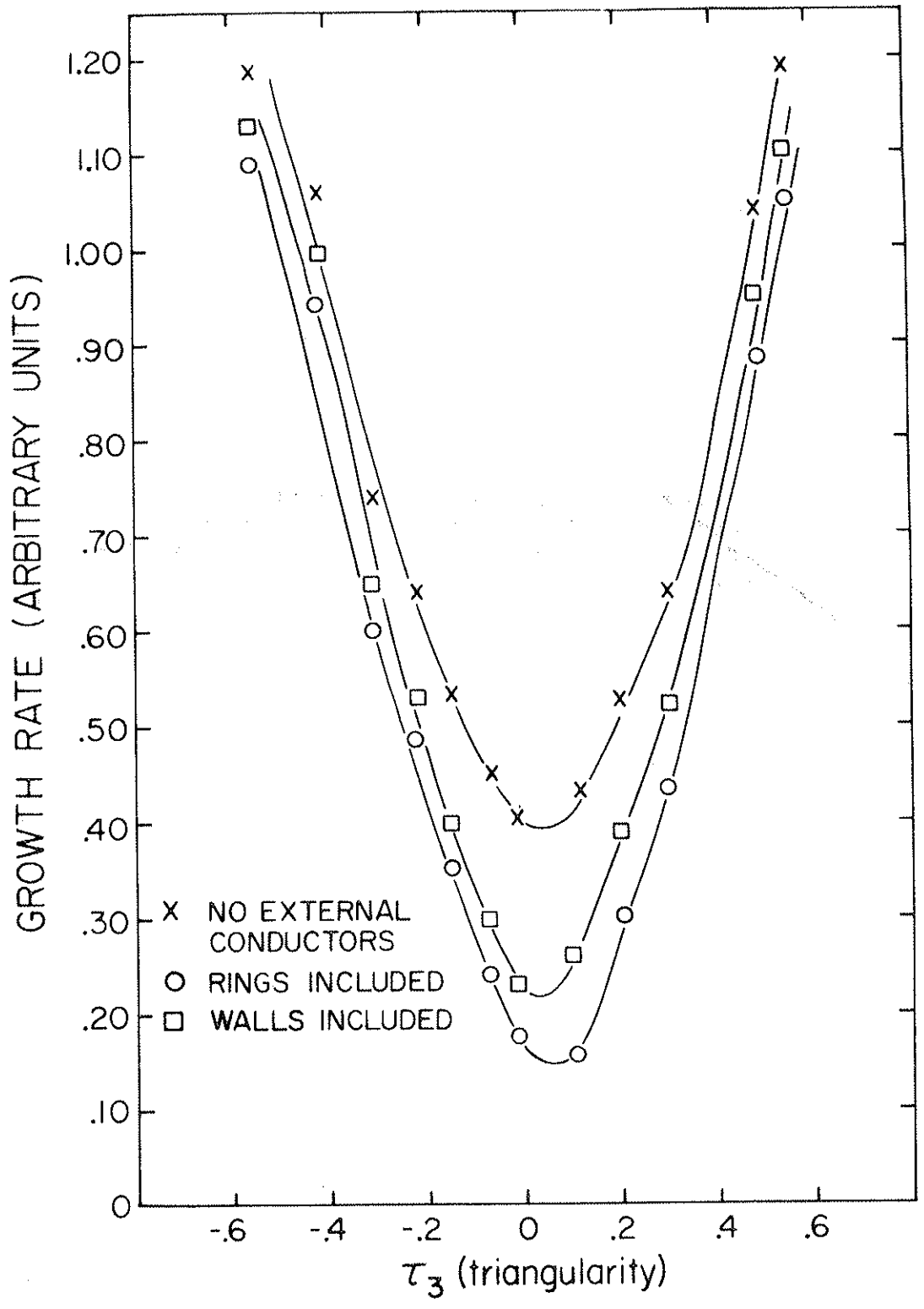
Figure 20: Theoretical vertical growth rates vs. T_3 for PDX as predicted by the PEST and PATENT codes without passive stabilization.
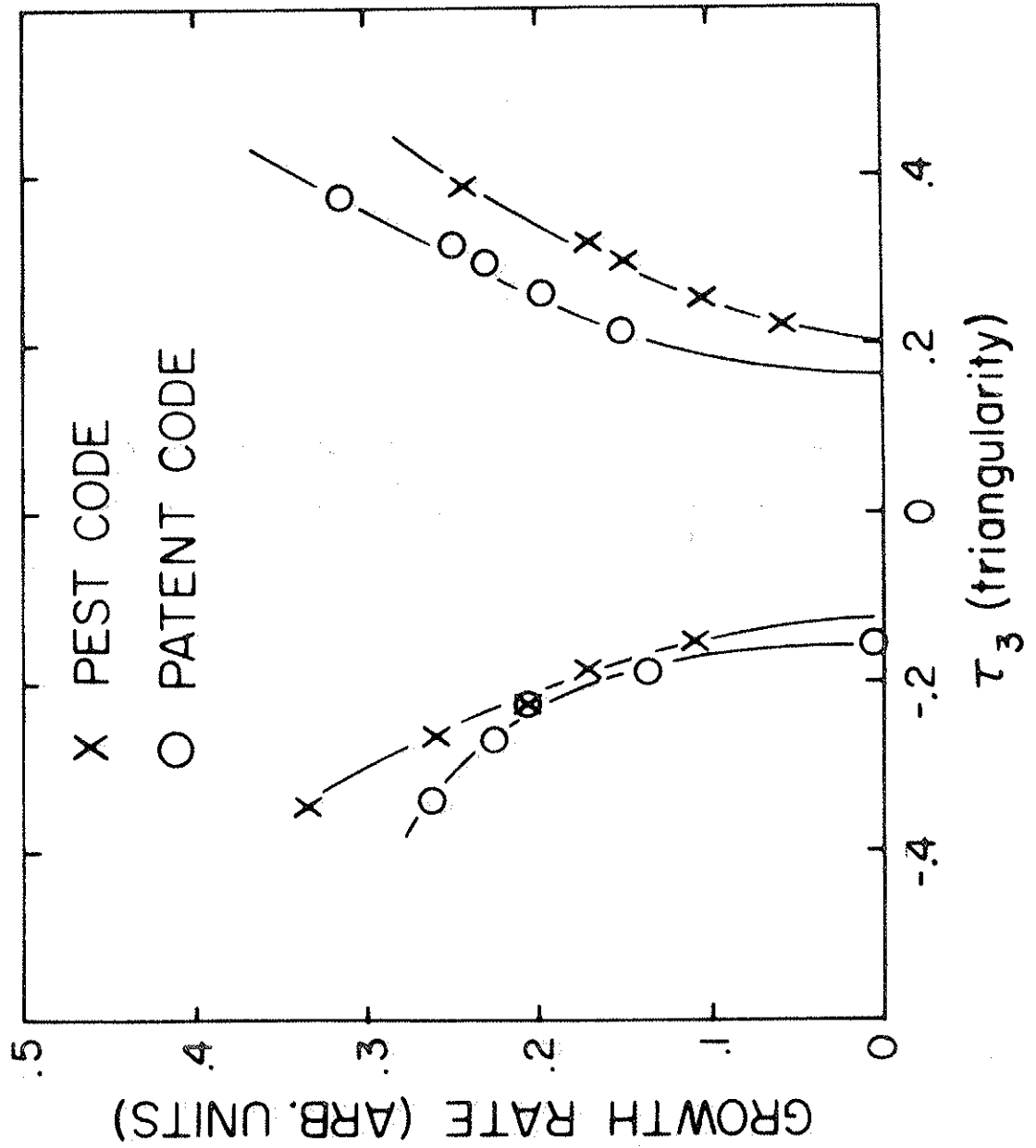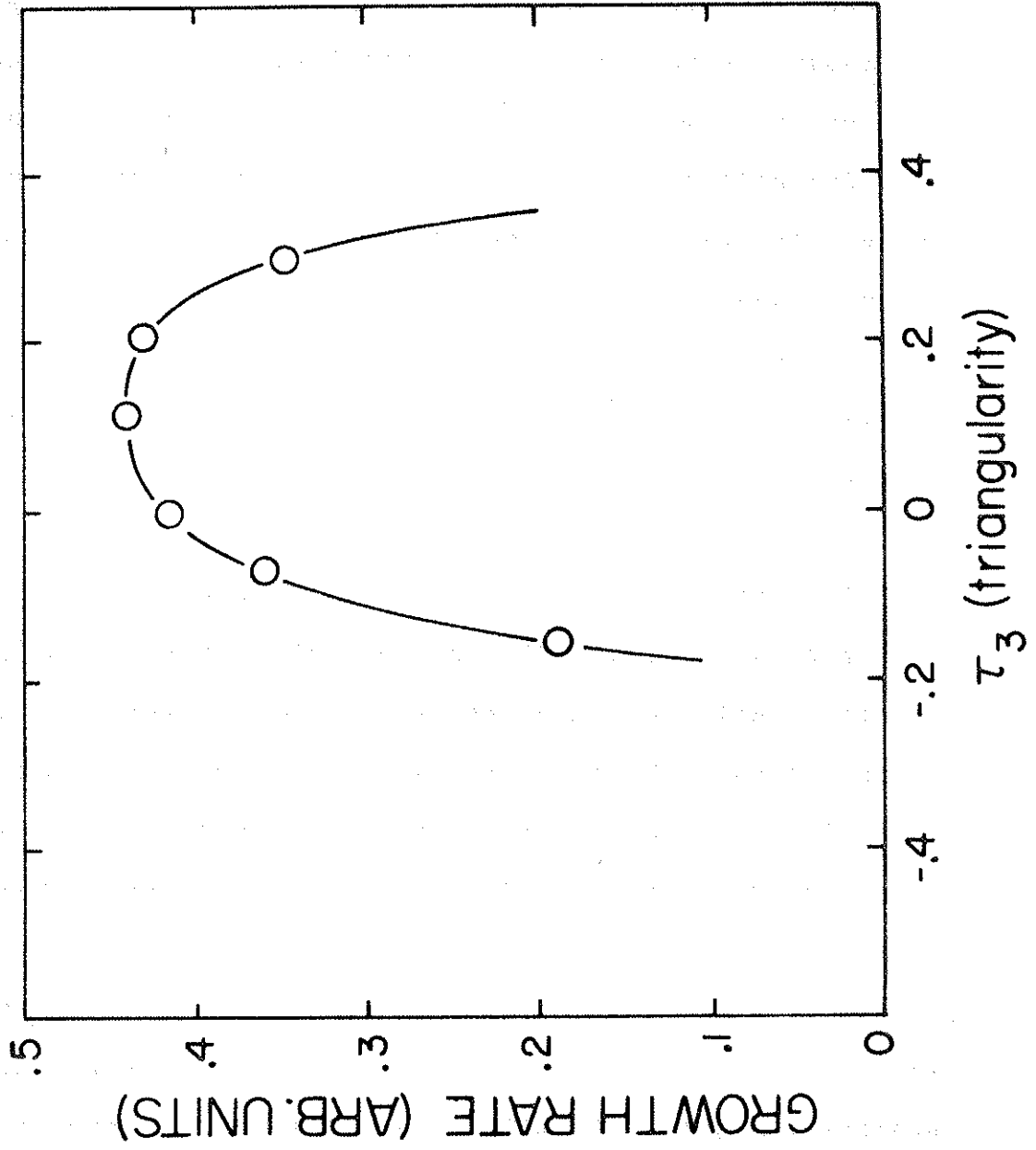
Figure 21: Theoretical horizontal growth
rates vs. T_3 for the Tokapole, as
predicted by PEST, without passive
stabilization.

cross sections. The dependence of the instability growth rate on deeness (T_3) may now be observed. Ignoring the presence of rings and walls, figures 19 and 20 show that the square is more stable, vertically, than the dee or inverse-dee, which have roughly equal growth rates, for both Tokapole and PDX equilibria. These machines are quite different in geometry and size. In addition, the Tokapole has a flatter current profile than the parabolic shape predicted for PDX. It appears that the relative stability of different shaped cross sections is fairly machine independent.

The growth rates for PDX calculated by PATENT (figure 20) agree well with PEST. Using PATENT, the motion of the magnetic axis may be observed for different initial perturbations. It is seen (fig. 17) that if the axis is initially .02 minor radii above the midplane the plasma moves unstably upward. Equivalent positioning of the axis below the midplane produces downward motion. Initial and final pictures of an equilibrium are shown in figure 18. The growth is exponential for excursions well into the nonlinear regime. Growth rates increase as the initial position of the magnetic axis is moved farther from the midplane (fig. 22). For an initial vertical position of

Figure 22: Theoretical predictions of the
nonlinear code (PATENT) for growth rate
as a function of perturbation.
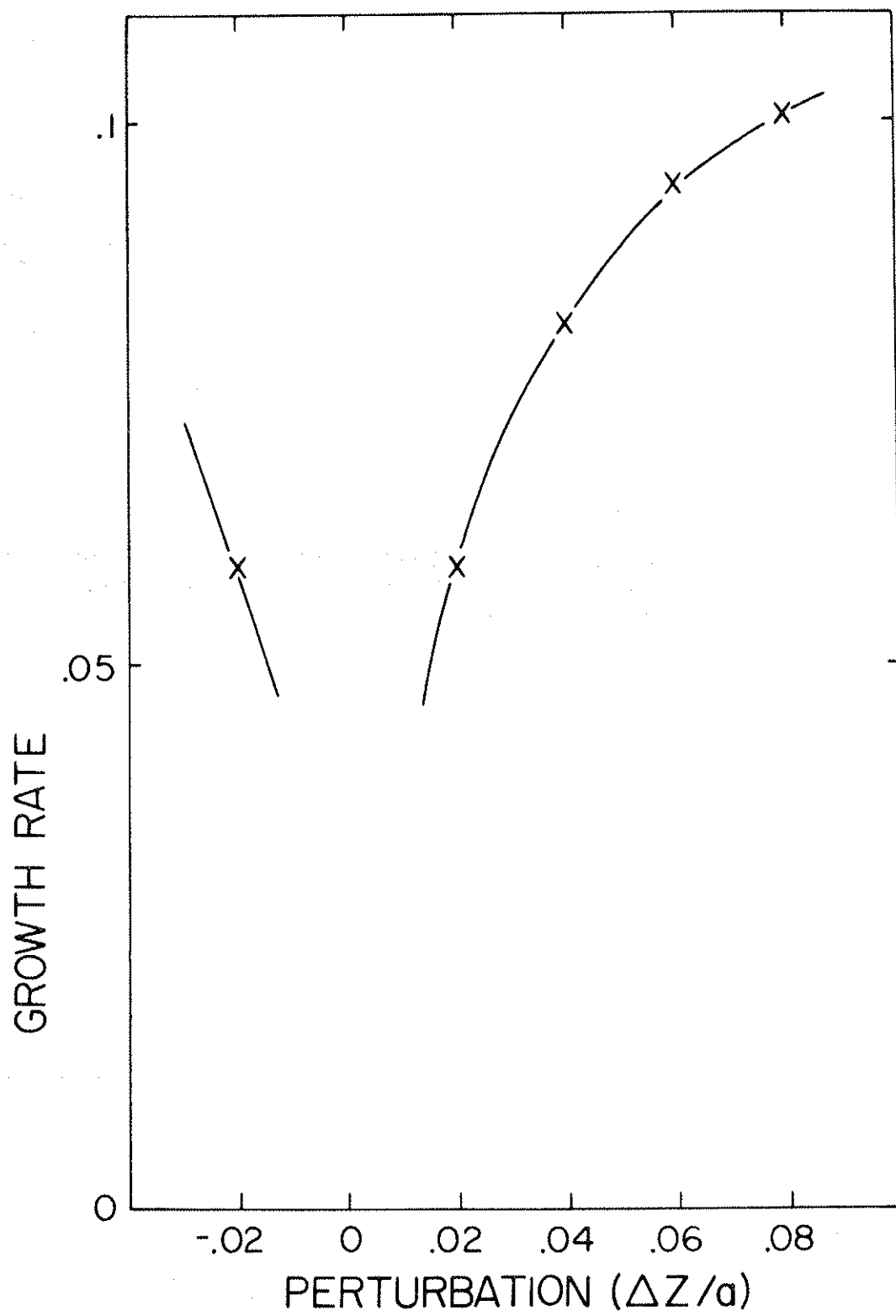
the magnetic axis on the midplane, the axis oscillates about that starting point.

The effect of the toroidal field on instability growth was found to be minimal. An order of magnitude difference in the toroidal field produced only a .5% change in growth rate; stability was enhanced for inverse-dee's ($T_3 > 0$), degraded for dee's ($T_3 < 0$). This difference is perhaps related to the $\underline{J}_{pol} \times \underline{B}_{tor}$ force which points outward from the plasma center (see section I.B). As the unstable dee ($T_3 < 0$) moves inward in major radius to higher B_{tor}, the force increases thereby encouraging unstable motion. For the inverse-dee ($T_3 > 0$) the motion is outward and the effect of the toroidal field is opposite.

Stability to horizontal axisymmetric displacements of Tokapole and PDX equilibria was studied using PEST. For Tokapole equilibria, the square and other shapes of small $|T_3|$, were found to be horizontally unstable with the square having the highest growth rate (fig. 21). During horizontal motion the midplane forces due to the vertical field are stabilizing whereas the vertical extremities experience the destabilizing presence of the x-points. Thus, the dee's, which are more heavily weighted in area towards the stabilizing midplane, are relatively more

stable than the square. Examination of figure 21 reveals

the dee to be relatively more stable than the inverse-dee

to horizontal motion. We consider this result to be due

to the toroidal nature of a tokamak; most likely the self

expansive force of the plasma current.   For sufficiently

large $|T_3|$ both Tokapole and PDX equilbria were found to

be horizontally stable.

F. Results With Passive Feedback

Both codes can be used to assess the role of passive

conductors surrounding the plasma.   In the case of the

PEST code, any combination of conductors (walls and/or

rings) can be included and their effect on the linear

growth is found by evaluating the inductive contribution

to the energy principle of Bernstein et al.[21,22,32].

Figure 19 shows the effect of adding either rings or

walls.   In the presence of both walls and rings all

Tokapole equilibria studied are stable except those of

extreme triangularity.   As can be seen from this same

figure, adding conductors has a greater effect on the

square than on other plasma cross sections. This may be

due to the square being in closer proximity to all four
rings or walls than shapes of larger $|T_3|$. The
stabilizing effect of the rings exceeds that of the walls
since the rings are closer to the plasma. The PATENT code
yielded similar results when used to evaluate the effect
of passive feedback due to rings.

CHAPTER IV

SUMMARY AND DISCUSSION

Previous experimental work[14-17] on the axisymmetric instability in noncircular tokamaks has, for the most part, inferred gross plasma motion from signals external to the plasma. Experimental results were compared with related theories in the literature through such parameters as ellipticity and/or averaged decay index, derived by modeling the plasma current as a filament[31]. In this experiment we can accurately observe the motion of the poloidal magnetic flux surfaces and the time evolution of internal parameters (J,q,E) through internal measurements. These experimental data are carefully compared to theoretical predictions of PEST, applied to this specific machine. The plasma cross section is characterized by ellipticity, triangularity and rectangularity parameters. A second code, PATENT, follows the nonlinear time development. This code is only applied to PDX geometry with shapes similar to Tokapole equilibria. Similar results, by PEST, for the two different machine geometries indicates our results are fairly machine independent.

Linear theory predicts that, in the absence of passive stabilization, all experimental equilibria are vertically unstable on the MHD time scale (T_a). However, the square is more stable than the dee or inverse-dee. This is consistent with the dee's being poloidally more asymmetric than the square; that is, the radius of curvature of the magnetic surface near the x-point is smallest for the dee's. Furthermore, only square-like equilibria are horizontally unstable. With the addition of passive feedback from rings and walls all equilibria are predicted to be stabilized with the greatest influence exerted by the rings. An experimental picture emerges in close agreement with theory, with modifications to account for the finite plasma resistivity limitation to the passive feedback. When the experimental plasma is z-symmetric both inside and outside dee's oscillate on the plasma resistive time scale. Thus, these equilibria are linearly unstable, as in theory without conductors, but are nonlinearly restored by passive feedback to a stable oscillation. Passive feedback does not linearly stabilize the equilibria; i.e. the plasma is displaced a finite amount before nonlinear feedback occurs. The complete stabilization of this mode by passive feedback, that the ideal MHD PEST code predicts, is not observed in the dee's since the finite plasma resistivity causes damping of the

induced stabilizing currents in the rings, plasma and walls. The square appears entirely stable vertically, implying that passive feedback is more effective for this shape as is also indicated theoretically in figure 19.

All evidence, both experimental and theoretical, indicates that the square is more stable than both dee's, which have similar stability properities. If the initial vertical position of the magnetic axis of both dee's is experimentally positioned above (below) the midplane they are linearly unstable. However, passive feedback is unable to reverse the vertical motion and the displacement grows exponentially with a growth time again on the order of the plasma L/R time (resistive decay time). The square is vertically stable, experimentally, even when positioned away from the midplane. The form of the vertical displacement of the dee's seen experimentally (fig. 9) or in the PATENT code (fig. 18) is a non-rigid deformation in the direction of the separatrix x-point. Also, in both this code and experiment, growth rate increases as the magnetic axis is positioned further above the midplane.

In the absence of vertical movement, a steady horizontal motion is experimentally evident. As the plasma travels horizontally it becomes increasingly

dee-shaped (increasing $|T_3|$) and eventually becomes vertically unstable. Indeed, PEST predicts this same horizontal instability for the square and other shapes of small $|T_3|$ (fig. 21).

A crucial factor absent in the codes used here, and in all published calculations, is the finite plasma resistivity. Seki[8] and Jardin[13] discuss only the finite conductivity of the external conductors. In our experiment the plasma resistive decay time may impose a bound on the instability growth time. When the plasma resistance is experimentally doubled, the instability growth rate also doubles. The correlation is not precise. Although the plasma shape remains approximately the same, a 1.5 cm. shrinkage in the plasma minor radius accompanies the resistance change. However, modeling of the effect of this change on the instability growth by PEST indicates that the minor radius decrease causes only a 4% increase in growth rate. The experimental and theoretical results of this paper are summarized in table 1.

Finally, the results presented here are not peculiar to the Tokapole machine or geometry for three reasons. Firstly, the Tokapole machine is up-down symmetric since

Table 1: Comparison of experiment and theory as predicted by the numerical stability codes.

TABLE

THEORY	EXPERIMENT
Vertical Stability:	
Dee and inverse dee linearly unstable without feedback.	Same.
Square linearly unstable without feedback.	Linear state undetectable-- square stable.
Square more stable than dee and inverse dee.	Same.
All shapes linearly stabilized by passive feedback.	Dee and inverse dee <u>not</u> linearly stabilized by passive feedback. All shapes can be <u>nonlinearly</u> stabilized by passive feedback.
$\tau_{growth} \sim \tau_{Alfvén}$, without feedback. stable, with feedback.	$\tau_{growth} \sim L/R\big|_{plasma}$ with feedback.
Nonlinear growth is exponential.	Same.
Nonlinear motion is nonrigid, toward separatrix field null.	Same.
Effect of plasma resistivity	τ_{growth} decreases with increasing plasma resistivity which limits effectiveness of feedback.
If magnetic axis is initially placed above, below or precisely on the midplane, the plasma correspondingly moves up, down or oscillates.	Same
Horizontal Stability:	
Squarelike plasmas are more unstable than dee and inverse dee.	Same.

the plasma shows no vertical preference in its motion. When initially positioned slightly above (below) the midplane the unstable motion is upward (downward). When centrally positioned it oscillates. Secondly, qualitative comparison of PEST predictions for Tokapole and PDX are very similar despite obvious machine differences. Thirdly, the wide seperation of the poloidal Alfven, growth and ring L/R times (T_g $\sim T_{L/R(plasma)}$ $\sim .05$ $T_{L/R(rings)}$ $\sim 10^3 T_a$) clearly indicates the determining factors of the growth rate.

IMPLICATIONS

With the knowledge that this thesis work has provided me, I'd like to discuss its implications. It seems, at this point in time, that tokamaks of the future will neccesarily have noncircular plasmas. It will be very important, when designing and running these machines (e.g. PDX, INTOR), to remember what problems this noncircularity can cause. The axisymmetric instability will not be the deciding factor in choosing what shape, dee vs. inverse-dee vs. square, to use. β-limits probably will be. But, this instability will be of prime importance in machine design and day to day running in that we must take

into account the characteristic decay times of the plasma and surrounding conductors.

BIBLIOGRAPHY

[1]Wesson, J.A., Nucl. Fusion 18 (1978), 87.

[2]Todd, A.M.M., et al., Nucl. Fusion 19 (1979), 743.

[3]Dobrott, D.R., & Miller, R.L., Phys. of Fluids 20 (1977), 1361.

[4]Rebhan, E., Nucl. Fusion 15 (1975), 277.

[5]Rebhan, E. and Salat A., Nucl. Fusion 16 (1976), 805.

[6]Rebhan, E. and Salat A., Nucl. Fusion 18 (1978), 1431.

[7]Fukuyama, A. et al., Japanese Journal of Applied Physics 14 (1975), 871.

[8]Seki, S. et al., Journal of Phys. Soc. of Japan 36 (1975), 1667.

[9]Bernard, L.C., Berger, D., Gruber, R., & Troyon, F., Nucl. Fusion 18 (1978), 1331.

[10]Rosen, M.D., Phys of Fluids 18 (1975), 482.

[11]Okabayashi, M. and Sheffield, G., Nucl. Fusion 14 (1974), 263.

[12]Becker, G. and Lackner, J., Plasma Physics and Controlled Nuclear Fusion Research (IAEA,Tokyo,1977), Vol. 1, 401.

[13]Jardin, S.C., Phys. of Fluids 21 (1978), 395.

[14]Wooton, A.J., Nucl. Fusion 18 (1978), 1161.

[15]Sakurai, K. et al., J. of Phys. Soc. of Japan 43 (1977), 731.

[16]Cima, G., Robinson, D.C., Thomas, C.L., Wooton, A.J., Plasma Physics and Controlled Nuclear Fusion Research (IAEA, Tokyo, 1977) Vol. 1, 335.

[17]Toyama, P. et al., ibid., 323.

[18]Biddle, A., et al., Nuclear Fusion in press.

[19] Lipschultz, B., Prager, S.C., Osborne, T.H., Sprott, J.C., & Phillips, M., Physical Review Letters 43 (1979), 36.

[20] Grimm, R.C., Greene, J.M., Johnson, J.L., in Methods in Computational Physics, Vol. 16 (Killeen, J., Ed.) Academic Press, New York (1976) 253.

[21] Dewar, R.L., Nucl. Fusion 18 (1978), 1541.

[22] Todd, A.M.M., submitted to Journal of Computational Physics.

[23] Jardin, S.C., Johnson, J.L., Greene, J.M., Grimm, R.C., Journal of Computational Physics 29 (1978), 101.

[24] Meade, D.M. et al. Plasma Physics and Controlled Nuclear Fusion Research (IAEA, Vienna, 1975) Vol. 1, 605.

[25] Sprott, J.C., University of Wisconsin Report PLP 712.

[26] Prager, S.C., Sprott, J.C., Osborne, T.H., & Miller, K., University of Wisconsin Report PLP 756.

[27] Fisher, R.K., et al. Physical Review Letters 39 (1977), 622.

[28] Bortnikov, V., et al. Fiz. Plazmy 1 (1975), 931 [Soviet J. Plasma Phys. 1 (1975), 508.].

[29] Bhatnagar, V., et al. Plasma Physics and Controlled Nuclear Fusion Research (IAEA, Tokyo, 1977) Vol. 1, p. 359.

[30] Solov'ev, L.S., Zh. Eksp. Teor. Fiz. 53 (1967), p. 626 [Soviet Physics JETP 26 (1968), 400].

[31] Yoshikawa, S., Physics of Fluids 7 (1964), 308.

[32] Bernstein, I.B., Frieman, E.A., Kruskal, M.D., & Kulsrud, R.M., Proc. Royal Society (London) 244A (1958) 17.

[33] Pellat, R., Laval, G., & Soule, J., Physics of Fluids 17 (1974), 835.

[34] Miller, R.L., Chu, M.C., Physics of Fluids 21 (1978), 817.

[35]Berger, D., Gruber, R., & Troyon, F., Paper C3, 2nd European Conf. on Comput. Physics, Garching (1976).

[36]Newcomb, W.A., Nuclear Fusion: 1962 Supplement, Part 2 (1962), 451.